Atmos. Chem. Phys., 9, 1479–1501, 2009
www.atmos-chem-phys.net/9/1479/2009/

Atmospheric Chemistry and Physics

Isoprene photooxidation: new insights into the production of acids and organic nitrates

F. Paulot[1], J. D. Crounse[2], H. G. Kjaergaard[3], J. H. Kroll[2,4], J. H. Seinfeld[1,2], and P. O. Wennberg[1,5]

[1]Department of Environmental Science and Engineering, California Institute of Technology, Pasadena, CA, USA
[2]Division of Chemistry and Chemical Engineering, California Institute of Technology, Pasadena, CA, USA
[3]Department of Chemistry, University of Otago, Dunedin, New Zealand
[4]Center for Aerosol and Cloud Chemistry, Aerodyne Inc., Billerica, MA, USA
[5]Division of Geophysical and Planetary Sciences, California Institute of Technology, Pasadena, CA, USA

Received: 10 June 2008 – Published in Atmos. Chem. Phys. Discuss.: 31 July 2008
Revised: 4 February 2009 – Accepted: 4 February 2009 – Published: 23 February 2009

Abstract. We describe a nearly explicit chemical mechanism for isoprene photooxidation guided by chamber studies that include time-resolved observation of an extensive suite of volatile compounds. We provide new constraints on the chemistry of the poorly-understood isoprene δ-hydroxy channels, which account for more than one third of the total isoprene carbon flux and a larger fraction of the nitrate yields. We show that the *cis* branch dominates the chemistry of the δ-hydroxy channel with less than 5% of the carbon following the *trans* branch. The modelled yield of isoprene nitrates is 12±3% with a large difference between the δ and β branches. The oxidation of these nitrates releases about 50% of the NO_x. Methacrolein nitrates (modelled yield ≃15±3% from methacrolein) and methylvinylketone nitrates (modelled yield ≃11±3% yield from methylvinylketone) are also observed. Propanone nitrate, produced with a yield of 1% from isoprene, appears to be the longest-lived nitrate formed in the total oxidation of isoprene. We find a large molar yield of formic acid and suggest a novel mechanism leading to its formation from the organic nitrates. Finally, the most important features of this mechanism are summarized in a condensed scheme appropriate for use in global chemical transport models.

Correspondence to: F. Paulot
(paulot@caltech.edu)

1 Introduction

Isoprene (2-methyl-1,3-butadiene, C_5H_8) is a short-lived compound ($\tau_{1/2}$=1−2 hours) emitted by many deciduous trees during daylight hours. Between 0.5% and 2% of the carbon fixed by isoprene emitting plants is released to the atmosphere as isoprene (Harley et al., 1999), a flux accounting for about one third of the total anthropogenic and natural volatile organic compounds (VOC) emissions (Guenther et al., 2006). Isoprene plays a crucial role in determining the oxidative chemistry of the troposphere. Ozone levels in urban as well as in rural sites are impacted by the sequestration and transport of NO_x via formation of isoprene nitrates (Horowitz et al., 1998) and various isoprene-derived peroxyacylnitrates. Moreover, field (Claeys et al., 2004) and chamber studies (Kroll et al., 2006; Surratt et al., 2006) have recently shown that compounds formed in isoprene photooxidation, such as methylglyceric acid or methylerythritol are ubiquitous in aerosol particles and may contribute significantly to the aerosol global burden (Henze and Seinfeld, 2006; van Donkelaar et al., 2007).

In the light of the potential for significant change in isoprene emissions due to climate and land use changes (Shallcross and Monks, 2000), studies have been made to predict the impact of altered isoprene emissions on tropospheric ozone (Sanderson et al., 2003; Wiedinmyer et al., 2006). von Kuhlmann et al. (2004) and Fiore et al. (2005) note, however, that quantifying this impact is difficult due to uncertainties regarding: 1) the dependence of isoprene emissions on temperature (Harley et al., 2004) and CO_2 concentration (Rosenstiel et al., 2003); and 2) the isoprene photooxidation

Published by Copernicus Publications on behalf of the European Geosciences Union.

scheme, especially the yields and fates of isoprene nitrates.

In this study, we use anion chemical ionization mass spectrometry (CIMS) to monitor the photooxidation of isoprene. This technique greatly expands the range of compounds that can be observed during the photooxidation of isoprene and other hydrocarbons (Ng et al., 2008). Quantitative interpretation is challenging, however, because 1) calibration standards are not available for many of the compounds identified and 2) mass analogs (compounds having the same mass) are not differentiated. Therefore the iterative development of a detailed mechanism is used to analyze the different signals and derive branching ratios and yields for the compounds identified.

First, we briefly describe the experiment emphasizing the calibration of CIMS measurements. Next, we report and identify the largest signals monitored by CIMS. We then discuss how these signals help constrain the development of the model emphasizing the δ-hydroxy channels, the organic nitrate yield and fate, as well as some routes to organic acids. Finally we discuss the potential implications of our findings for tropospheric chemistry and present a reduced mechanism suitable for inclusion in chemical transport model.

2 Experiment

2.1 Experimental setting

The data of the present study were collected in the 28 m^3 Caltech atmospheric chamber, in an experiment similar to those described by Kroll et al. (2006). Initial concentrations of isoprene, NO and H_2O_2 were 94 ppbv, 500 ppbv and 2.1 ppmv. The photolysis of H_2O_2 constitutes the primary OH source in the experiment. NO was added prior to isoprene so that the chamber was initially ozone free. The initial relative humidity was less than 6% and is assumed to be constant in this study. The temperature increased by about 5 degrees in the first one hundred minutes and remained constant thereafter at 296.5 K . To simplify modelling, we consider this temperature to hold during the whole experiment.

Isoprene decay was monitored using GC-FID. Ozone was measured by UV absorption (Horiba) and NO and NO_2 (after conversion to NO) by chemiluminescence. The size distribution and the volume concentration of secondary organic aerosol (SOA) were measured using a differential mobility analyzer (DMA, TSI 3760). Further details are available in Kroll et al. (2006).

2.2 CIMS

Gas-phase products were monitored using a novel CIMS technique (Crounse et al., 2006) with CF_3O^- as the reagent anion. Non reactive with ozone, carbon dioxide and dioxygen (Huey et al., 1996), CF_3O^- is a versatile reagent ion suitable for the study of many oxygenated compounds. In general, two primary ionization pathways are observed:

$$\mathrm{VOC} + \mathrm{CF_3O^-} \rightarrow \mathrm{VOC^-_{-H}{\cdot}HF} + \mathrm{CF_2O} \quad \text{(R1)}$$

$$\mathrm{VOC} + \mathrm{CF_3O^-} \leftrightarrows \mathrm{VOC{\cdot}CF_3O^-} \quad \text{(R2)}$$

A minor ionization pathway is observed for certain compounds:

$$\mathrm{CF_3O^-} + \mathrm{HOOX(O)R} \rightarrow \mathrm{HF} + \mathrm{CF_2O{\cdot}OOX(O)R^-} \quad \text{(R3)}$$

In Reaction (R3), CF_2O is incorporated into the original neutral molecule. Reaction (R3) has been observed for peroxynitric acid (PNA) and for peroxy acetic acid (PAA). While Reaction (R3) is not the major ionization pathway, in several cases it is useful for distinguishing certain mass analogs.

The dominant ionization pathway for an analyte depends mostly on the acidity (or fluoride affinity) of the neutral species (Amelynck et al., 2000; Crounse et al., 2006). Highly acidic compounds, such as nitric acid, only form the transfer product ion through Reaction (R1) while hydrogen peroxide and methylhydrogen peroxide (MHP) form only the cluster product ions through Reaction (R2). Species with intermediate acidity (e.g. formic and acetic acids) form both the transfer and cluster products. Most of the VOC measured in this study follow Reaction (R2).

In this study, air was drawn from the chamber through a perfluoroalkoxy Teflon line of 1.2 m length and 0.635 cm outer diameter (OD), at a rate of 10 standard liters per minute (slm), and then sub-sampled into the CIMS flow tube using a critical orifice made of glass. The orifice constrained the flow from the chamber into the CIMS to be 145 standard cubic centimeters per minute (sccm). Upon introduction to the CIMS flow tube, the chamber gas was diluted with 1760 sccm of UHP N_2 (99.999%) to a total pressure of 35 hPa, primarily to reduce the concentration of H_2O_2 to manageable levels. The gas is expanded in a flow tube (17.8 cm, 2.54 cm OD Pyrex glass coated with a thin layer of Teflon (Fluoropel 801A, from Cytonix Corp.)) before reacted with a transverse ion beam of the reagent anion (Crounse et al., 2006, Fig. 1).

Mass scans were conducted using a quadrupole mass spectrometer from m/z=18 to m/z=275 dwelling on each mass for 1 s (giving a scan cycle of about $4\frac{1}{2}$ min). The mass scans were repeated throughout the duration of the experiment (17 h). Zero scans were conducted periodically throughout the experiment by overfilling the critical orifice on the high pressure (chamber) side with UHP N_2. In addition to providing instrumental backgrounds, the temporal response of the zero scans give insight into the strength of the interaction of the measured compounds with the equipment walls.

The instrumental background signals for most of the large molecular weight products produced in isoprene oxidation are very small (after the instrument has been sampling clean zero air for an extended period of time), which suggests that variations in instrumental background over the course

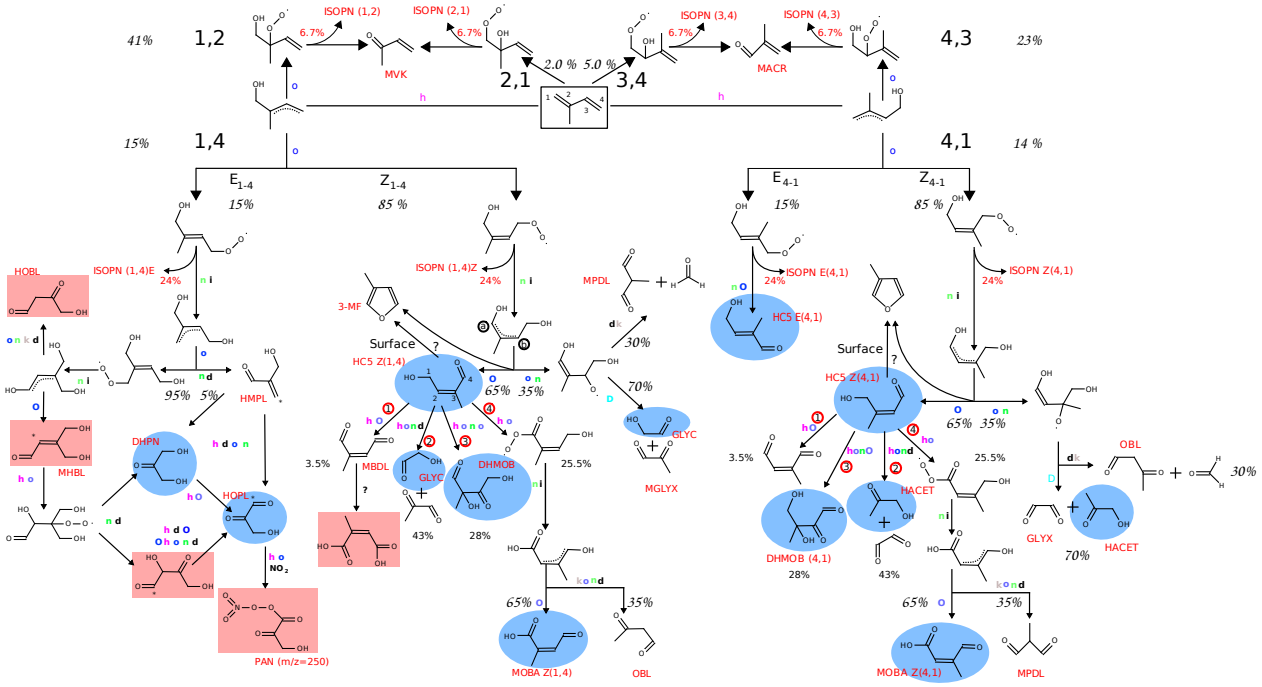

Fig. 1. Summary of the most prevalent first steps of isoprene photooxidation under high NO_x conditions. Abbreviations: i: δ_1^5 isomerization−Reaction (R16), h: OH+VOC (abstraction or addition) $*$ denotes the location of the reaction, o: $R + O_2 \rightarrow RO_2$, O: Reaction (R15), D: Dibble mechanism (cf. Section 4.1.1), n: $RO_2 + NO-$ Reaction (R7), d: decomposition - Reaction (R14), k: keto-enol tautomerism (possibly due to heterogeneous enol/ketone conversion). Blue circles: detected and correctly captured by the model. Red square: Insufficient data/model discrepancy.

of the experiment are not important for these signals. Compounds with a smaller molecular weight (e.g. formic and acetic acids) do have instrumental backgrounds, but the level of the instrumental background is small relative to the signal generated in the isoprene oxidation experiment (more than 10 times smaller), so ignoring instrumental background changes over the course of the experiment for these species does not introduce a substantial error.

2.3 Calibration

The concentration of a compound X, whose product ion is detected at m/z=p, is calculated through:

$$[X]_{\text{ppbv}} = \frac{\widehat{\text{Signal}(m/z\text{=p})}}{c_X} \quad (1)$$

where $\widehat{\text{Signal}(m/z\text{=p})}$ is the normalized signal associated with X (cf. Appendix B1) and c_X is the calibration constant for the compound X in ppbv^{-1}.

In many cases, no standard is readily available and no experimental determination of c_X can be made. In such cases, we assume that c_X is related to the thermal capture rate (k_X) and the binding energy of the cluster. k_X is estimated from the Langevin-Gioumousis-Stevenson-based collision rate. We use the empirical approach developed by Su and Chesnavich (1982) to calculate k_X from the dipole moment (μ_X) and the polarizability (α_X) of X.

In the absence of experimental determinations of μ_X and α_X, we use quantum chemical calculations to estimate them. The lowest energy conformers of the molecules are found with the conformer searches method within the Spartan06 quantum package (Wavefunction Inc., 2006) at the B3LYP/6-31G(d) level of theory. The dipole moments and static polarizabilities are then calculated for the optimized geometries at the same level of theory. When a molecule has several low energy conformers, a thermally-weighted average of their reaction rate coefficients is used for k_X (cf. Appendix B2 for details).

The sensitivity of the instrument to X also depends on the binding energy between X and the reagent anion as well as the nature of the reagent anion. In the presence of abundant ligands (L) such as water or hydrogen peroxide, the sensitivity of the CIMS to some VOC is modified through two different processes: 1) $CF_3O^- \cdot L$ may react faster with X than the bare CF_3O^- anion because ligand exchange reactions can stabilize the product ion to a greater extent; 2) the cluster $CF_3O^- \cdot L$ may be sufficiently stable leading to a lower sensitivity at higher L mixing ratio due to ligand exchange:

Table 1. Signals monitored by Chemical Ionization Mass Spectrometry. $\mathcal{C}$ denotes a cluster (Reaction (R2)) and $\mathcal{T}$ a transfer (Reaction (R1)). Uncertain identifications (cf. text) are highlighted by a $\star$.

m/z	Nature	Attribution	Formula	CAS
Organic				
65	$\mathcal{T}$	Formic Acid	CH_2O_2	64-18-6
79	$\mathcal{T}$	Acetic Acid	$C_2H_4O_2$	64-19-7
107	$\mathcal{T}$	Pyruvic Acid*	$C_3H_4O_3$	127-17-3
131	$\mathcal{C}$	Formic Acid	CH_2O_2	64-18-6
133	$\mathcal{C}$	MHP	CH_4O_2	3031-73-0
133	$\mathcal{T}$	MOBA Z(1,4)	$C_5H_6O_3$	63170-47-8
133	$\mathcal{T}$	MOBA Z(4,1)	$C_5H_6O_3$	70143-04-3
145	$\mathcal{C}$	Acetic Acid	$C_2H_4O_2$	64-19-7
145	$\mathcal{C}$	GLYC	$C_2H_6O_2$	141-46-8
159	$\mathcal{C}$	HACET	$C_3H_6O_2$	116-09-6
161	$\mathcal{C}$	PAA	$C_2H_4O_3$	116-09-6
169	$\mathcal{C}$	HMHP	CH_4O_3	15932-89-5
173	$\mathcal{C}$	HOPL*	$C_3H_4O_3$	997-10-4
173	$\mathcal{C}$	Pyruvic Acid*	$C_3H_4O_3$	127-17-3
175	$\mathcal{C}$	DHPN	$C_3H_6O_3$	96-26-4
185	$\mathcal{C}$	HC5 E(4,1)	$C_5H_8O_2$	
185	$\mathcal{C}$	HC5 Z(1,4)	$C_5H_8O_2$	519148-47-1
185	$\mathcal{C}$	HC5 Z(4,1)	$C_5H_8O_2$	519148-44-8
189	$\mathcal{C}$	DHB	$C_4H_8O_3$	57011-15-1
190	$\mathcal{C}$	ETHLN	$C_2H_3NO_4$	72673-15-5
199	$\mathcal{C}$	MOBA Z(1,4)	$C_5H_6O_3$	63170-47-8
199	$\mathcal{C}$	MOBA Z(4,1)	$C_5H_6O_3$	70143-04-3
201	$\mathcal{C}$	MHBL*	$C_5H_8O_3$	
204	$\mathcal{C}$	PROPNN	$C_3H_5NO_4$	6745-71-7
217	$\mathcal{C}$	DHMOB (1,4)	$C_5H_8O_4$	
217	$\mathcal{C}$	DHMOB (4,1)	$C_5H_8O_4$	
232	$\mathcal{C}$	ISOPN (1,2)	$C_5H_9NO_4$	227607-01-4
232	$\mathcal{C}$	ISOPN (1,4) Z	$C_5H_9NO_4$	227606-97-5
232	$\mathcal{C}$	ISOPN (1,4) E	$C_5H_9NO_4$	227606-98-6
232	$\mathcal{C}$	ISOPN (2,1)	$C_5H_9NO_4$	227607-02-5
232	$\mathcal{C}$	ISOPN (3,4)	$C_5H_9NO_4$	601487-80-3
232	$\mathcal{C}$	ISOPN (4,1) Z	$C_5H_9NO_4$	227606-99-7
232	$\mathcal{C}$	ISOPN (4,1) E	$C_5H_9NO_4$	227607-00-3
232	$\mathcal{C}$	ISOPN (4,3)	$C_5H_9NO_4$	227606-96-4
234	$\mathcal{C}$	MACRN	$C_4H_7NO_5$	
234	$\mathcal{C}$	MACRN (m)	$C_4H_7NO_5$	
234	$\mathcal{C}$	MVKN	$C_4H_7NO_5$	
234	$\mathcal{C}$	MVKN (m)	$C_4H_7NO_5$	
Inorganic				
62		NO_3^- (proxy for N_2O_5)		14797-55-8
66	$\mathcal{T}$	HONO		7782-77-6
82	$\mathcal{T}$	HNO_3		7697-37-2
98	$\mathcal{T}$	HO_2NO_2		26404-66-0
119	$\mathcal{C}$	H_2O_2		7722-84-1
132	$\mathcal{C}$	HONO		7782-77-6
148	$\mathcal{C}$	HNO_3		7697-37-2
164	$\mathcal{C}$	HO_2NO_2		26404-66-0

$$\mathrm{VOC.CF_3O^-} + L \leftrightarrows \mathrm{VOC} + \mathrm{L{\cdot}CF_3O^-} \quad \text{(R4)}$$
$$\mathrm{L} = \mathrm{H_2O}, \mathrm{H_2O_2}$$

For example, Crounse et al. (2006) reported that the sensitivity to methylhydroperoxide (MHP) decreases with the water vapor mixing ratio due to Reaction (R4).

In general large molecules featuring several functional groups (peroxide, nitrooxy, alcohol, carbonyl) exhibit only a weak dependence on the amount of water. Therefore, we neglect the binding energy effect in this study and take:

$$c_X = \frac{k_X}{k_{\mathrm{HNO_3}}} c_{\mathrm{HNO_3}} \quad (2)$$

where $k_{\mathrm{HNO_3}}$=1.93×10^{-9} cm^3 molecule^{-1} s^{-1} is calculated using the experimental dipole and polarizability of nitric acid and $c_{\mathrm{HNO_3}}$ is the sensitivity to nitric acid for typical conditions where the flow tube was operated (water vapor mixing ratio=150 ppmv). HNO_3 is used as the calibration reference because of the weak dependence of the sensitivity with water and its thorough laboratory study (Huey et al., 1996; Amelynck et al., 2000; Crounse et al., 2006).

When several compounds are observed at the same m/z, we report the signal calibrated with a reference calibration c_{ref} and the modeled concentrations of each compound X_i multiplied by s_{X_i}=c_{X_i}/c_{ref}, so that one can compare measured signal with the prediction of the mechanism. The predicted concentration of a specific compound is therefore $[X_i]_{\mathrm{calibrated\ model}}/s_{X_i}$.

Finally, molecules such as isoprene, methacrolein (MACR), methylvinylketone (MVK) or peroxyacylnitrate (PAN) are not observed with our measurement technique despite their relatively large dipole moment. More generally, the method is not sensitive to simple aldehydes, alcohols, and ketones, presumably due to the low binding energy of these compounds with CF_3O^-.

3 Results

After the photolysis lights are turned on, isoprene decays with a half life of ∼20 min (Fig. A3). Several inorganic markers of the chemical evolution of the system can be monitored by CIMS (Table 1 and Fig. A4). Nitrous acid (transfer at m/z=66, cluster at m/z=132, Fig. A4), peaks after 50 min and has mostly disappeared after 150 min. HONO is associated with a very large concentration of NO which defines our first chemical regime ($0 \leq t \leq 150$ min). Given the high concentration of NO, little ozone is formed and isoprene photooxidation proceeds almost entirely through OH addition. Pernitric acid (PNA, transfer at m/z=98, cluster at m/z=164, Fig. A4) grows steadily peaking at ∼600 min. Given the sensitivity of PNA to the ratio HO_2:NO_2, the time when PNA reaches its maximum indicates the transition from a NO_x

(Regime 2: $150 \leq t \leq 600$ min) to a HO_x-dominated chemistry (Regime 3: $t \geq 600$ min). In this study, we focus on the NO_x-dominated chemistry, limiting our discussion to the first and second regimes. Studies of low NO_x chemistry will follow in a separate manuscript. Nitric acid (transfer at m/z=82) grows steadily during the experiment to reach ~430 ppb at the end of the experiment. We estimate dinitrogen pentoxide profile by removing the nitric acid contribution to the NO_3^- (m/z=62) temporal signal (Huey et al., 1996). The corrected signal exhibits a shape similar to PNA, peaking after ~500 min at ~ 3ppb.

In Table 1 and Figs. 1 to 15, we report the main signals measured by CIMS, the chemical formula of the associated compounds as well as their most likely identification using mechanistic considerations. To our knowledge, this is the first time that the temporal evolutions of isoprene nitrates (cluster at m/z=232, Fig. 9) and methacrolein/methylvinylketone nitrates (cluster at m/z=234, Fig. 13) have been monitored. We also observe the formation of small carboxilic acids such as formic and acetic acid, which can be clearly identified given that they undergo both Reactions (R1) and (R2). This specificity helps identify larger acidic compounds such as (Z)-2/3-methyl-4-oxobut-2-enoic acid (MOBA): the signal recorded at m/z=199 (cluster) correlates with the associated transfer at m/z=133 (ρ=0.93 for the first 400 min). This also allows differentiation of certain mass analogs, e.g. the contribution of acetic acid cluster to m/z=145 can be removed using its experimental ratio between transfer and cluster. The residual is the cluster of glycolaldehyde (m/z=145).

Unfortunately most mass analogs, such as isoprene nitrates (m/z=232) are positional isomers, and thus cannot be specifically identified using this approach, thus precluding the derivation of their concentrations. To overcome this difficulty, a detailed mechanism has been developed iteratively using the constraints of organic and inorganic signals in association with previously identified mechanisms (Appendix A).

4 Discussion

4.1 δ-hydroxy channels

Under chamber experimental conditions, isoprene photooxidation proceeds primarily through the addition of OH to the two double bonds (position 1, 2, 3 and 4, in Fig. 1). In the following we will denote the different channels by the couple (i, j), where i and j refer, respectively, to the carbon on which the HO and O_2 addition occurs. Besides β-hydroxy peroxy radicals (1, 2) and (4, 3), additions to positions 1 and 4 can lead, after addition of O_2, to four δ-hydroxy peroxy radicals (Sprengnether et al., 2002), referred to as $Z_{1,4}$, $E_{1,4}$, $Z_{4,1}$, $E_{4,1}$. The branching ratio between these different channels remain uncertain (cf. Sect. C1). Here we use a combination of theoretical (Lei et al., 2000) and experimental results (Sprengnether et al. (2002) and this study) as constraints: $Y_{1,2} \simeq 41\%$, $Y_{1,4} \simeq 15\%$, $Y_{2,1} \simeq 2\%$, $Y_{4,3} \simeq 23\%$, $Y_{4,1} \simeq 14\%$, $Y_{3,4} \simeq 5\%$.

As most studies of isoprene photooxidation have focused on the main decomposition channels (1, 2 and 4, 3) yielding MACR and MVK (Paulson et al., 1992; Sprengnether et al., 2002; Karl et al., 2006), the δ-hydroxy channels, which account for about 30% of the carbon and a large fraction of the organic nitrates, remain poorly constrained. A large number of products originating from the δ-hydroxy channels can be monitored by CIMS which motivates our emphasis on their chemistry.

4.1.1 Chemistry of the δ-hydroxy channels

$Z_{1,4}$. The reaction of the peroxy radical with NO yields an alkoxy radical which undergoes a δ_1^5 isomerization (Atkinson, 1997; Park et al., 2004). The resulting β-hydroxy allyl radical can then react with O_2 and form a 1,4-hydroxycarbonyl, (2Z)-4-hydroxy-2-methylbut-2-enal (HC5 Z(1,4)) detected as a cluster at m/z=185 (Fig. 2). The detection of its ^{13}C isotope at m/z=186 supports the attribution of the signal to HC5. Formation of glycolaldehyde (GLYC cluster at m/z=145, Fig. 3) and methylglyoxal (MGLYX) at this stage of the photooxidation have also been described by Dibble (2004a,b). This reaction is based on the stabilization of the alkoxy radical, reproduced below, through a double hydrogen bond which prevents its decomposition while enhancing a double hydrogen shift involving the hydrogen of the alcohol groups.

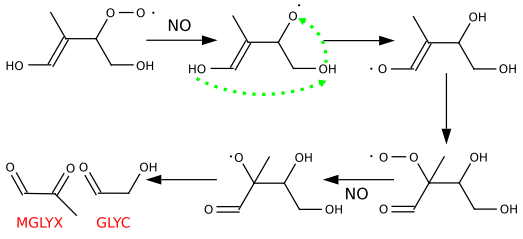

OH can add to the HC5 Z(1, 4) double bond (channels ② and ③ in Fig. 1), abstract the aldehydic hydrogen (channel ④) or the hydrogen α to the alcohol (channel ①). Addition on position ② is expected to yield GLYC and MGLYX. The signal detected at m/z=217 (Fig. 4) suggests the existence of channel ③. In this pathway the alkoxy radical formed after addition of OH on position 3 is stabilized enough by a double hydrogen bond, so that reaction of O_2 becomes competitive with unimolecular decomposition. This mechanism yields 2,4-dihydroxy-2-methyl-3-oxobutanal (DHMOB (1, 4)).

The signal recorded at m/z=199 correlates well (ρ=0.93 for the first 400 min) with the one at m/z=133. This correlation between a cluster and a transfer is usually associated with an acid functional group (cf. Sect. 2.2), which supports the formation of (Z)-2-methyl-4-oxobut-2-enoic acid (MOBA Z(1, 4)), a five carbon acid, from HC5 through channel ④ (Fig. 5).

$E_{1,4}$. The isomerization of the initial alkoxy radical can yield 2-(hydroxymethyl)prop-2-enal (HMPL) after reaction with O_2. A second isomerization would yield 4-hydroxy-3-oxobutanal (HOBL)

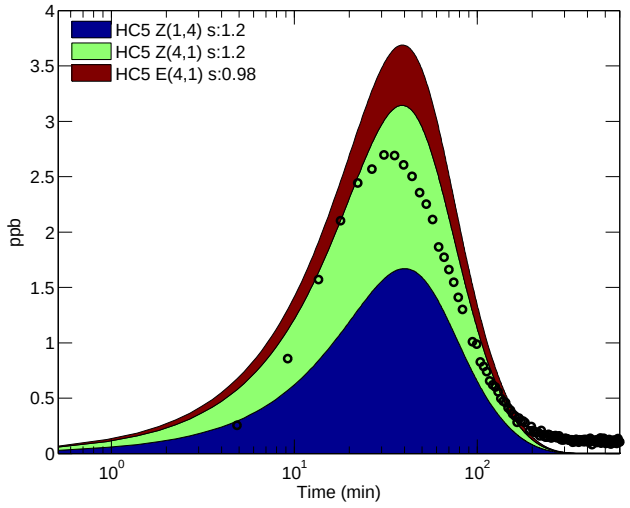

Fig. 2. Signal recorded at m/z=185 (black circles) and modeled HC5=HC5 Z(1,4)+HC5 Z(4,1) + HC5 E(4,1) (monitored as a cluster).

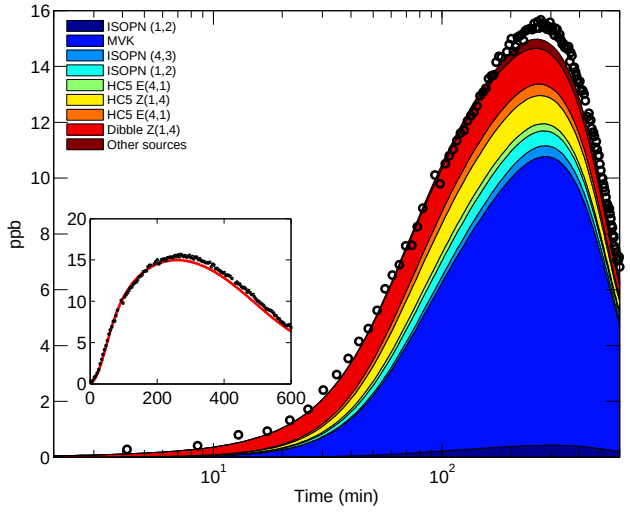

Fig. 3. Signal recorded at m/z=145 (black circles) compared with modeled GLYC profile. The contribution of acetic acid cluster has been removed using acetic acid transfer at m/z=79. Colored bars indicate the instantaneous modeled contributions of the different sources of GLYC.

or 4-hydroxy-3-(hydroxymethyl)but-2-enal (MHBL). The further photooxidation of HMPL and MHBL is expected to yield mainly dihydroxypropanone (DHPN), whose CF_3O^- cluster is observed at m/z=175 (Fig. 6), and hydroxyoxopropanal (HOPL, cluster at m/z=173 with pyruvic acid).

The reaction of OH with HOPL is expected to yield an acylperoxy radical which can further react with NO_2 yielding a PAN-like compound, 3-hydroxy-oxo-peroxyacylnitrate (PAN 250). This compound may be associated with the signal monitored at m/z=250, although the identification is not certain.

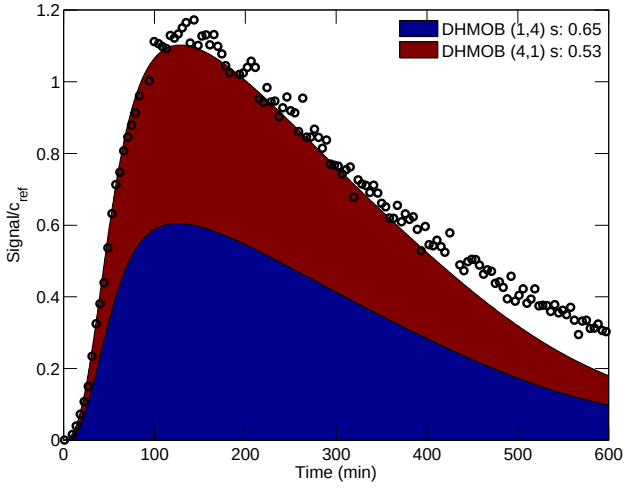

Fig. 4. Signal recorded at m/z=217 (black circles) and modeled DHMOB=DHMOB(1, 4) + DHMOB(4, 1) (monitored as a cluster).

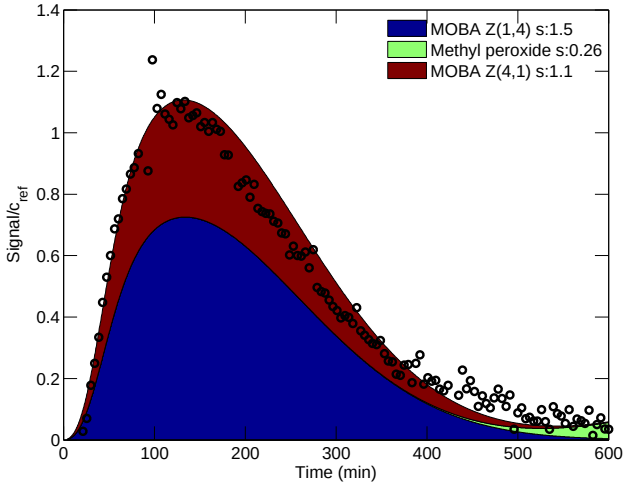

Fig. 5. Sum of the signals recorded at m/z=133 and m/z=199 (black circles) compared with MOBA=MOBA Z(1,4)+MOBA Z(4,1) (m/z=133 (transfer)+199 (cluster)) and MHP (cluster at m/z=133).

Signals originating from the E branch are much smaller than those originating from its Z counterpart. This suggests a large asymmetry between the E and Z δ-hydroxy channels.

Due to the similarity between the (4, 1) and (1, 4) branch, we only address the major differences.

$Z_{4,1}$. Hydroxyacetone (HACET, cluster at m/z=159, Fig. 7) and glyoxal (GLYX) can be formed from the decomposition of HC5 Z(4, 1) and HC5 E(4, 1). Similar to the formation mechanism of DHMOB(1, 4), the addition of OH to the less preferred position of HC5 Z(4, 1) (and E(4, 1)) is expected to yield 3,4-dihydroxy-3-methyl-2-oxobutanal referred to as DHMOB(4, 1) (Fig. 4).

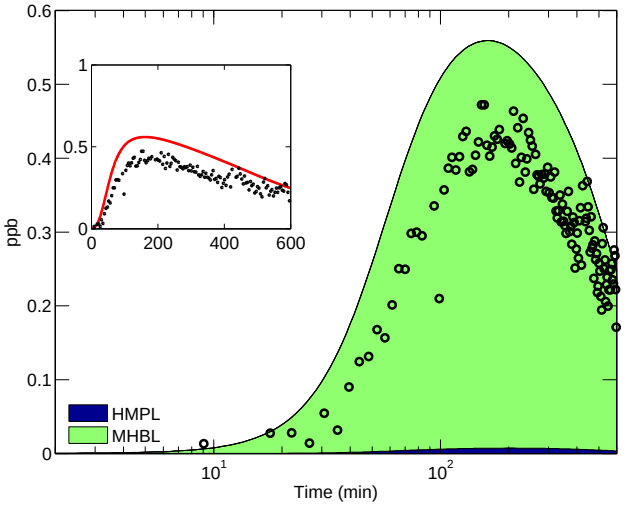

Fig. 6. Signal recorded at m/z=175 (black circles) compared to modeled DHPN (measured as a cluster).

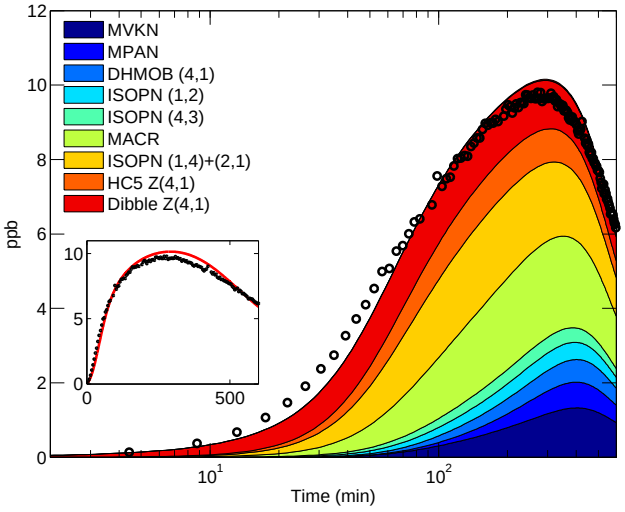

Fig. 7. Signal recorded at m/z=159 (black circles) compared with modeled HACET profile. Colored bars indicate the instantaneous modeled contributions of the different sources of HACET. MPAN source has been described by Orlando et al. (2002).

$E_{4,1}$. The alkoxy radical configuration prevents δ_1^5 isomerization (Reaction R16) and slows down its decomposition (Reaction R14). Therefore it is expected to react entirely with O_2 (Reaction R15) to yield a HC5 isomer (HC5 E(4, 1)).

4.1.2 Consequences

The observations of numerous compounds formed at different stages of δ-hydroxy pathways lead to several inferences about the general mechanism:

Channel asymmetry. If an equal partitioning of the carbon is assumed between $E_{1,4}$ and $Z_{1,4}$ as suggested by the theoretical work of Dibble (2002), the concentrations of both HOPL and DHPN are greatly overestimated while the concentrations of HC5=HC5 Z(1, 4)+HC5 E(4, 1)+HC5 Z(4, 1) and its products (DHMOB, MOBA) are underestimated. Good agreement with the observations is obtained when,

$$\frac{Y_{E_{1,4}}}{Y_{Z_{1,4}}} = \frac{15}{85} \quad (3)$$

An additional piece of evidence suggesting that little flux of carbon occurs through $E_{1,4}$ is the low signal recorded at m/z=201, which should include 3-methylhydroxy-4-hydroxybutenal (MHBL) based on its structural similarity with HC5. We use k_{OH}=6.13×10^{-12} cm^3 molecule^{-1} s^{-1} for DHPN (25% more than the SAR estimate) and k_{OH}=2.23×10^{-11} cm^3 molecule^{-1} s^{-1} for HOPL in order to properly capture their measured temporal profiles (Fig. 6).

The asymmetry between Z/E isomers contradicts the conclusions drawn from quantum mechanical calculations (Dibble, 2002) as well as the assumption made by most kinetic models of isoprene photooxidation (Paulson and Seinfeld, 1992; Fan and Zhang, 2004).

The discrepancy with quantum mechanical calculations may be related to a difference in the reaction of the *cis*/*trans* radical with O_2. The radicals are formed with approximately 40 kcal/mol excess energy. The minimum isomerization barrier is estimated to be about 15 kcal/mol (Dibble, 2002). Therefore, assuming a collision stabilization of 100 cm^{-1}collision^{-1}, the radicals undergo nearly 100 collisions (20 with O_2) before they are cooled below the isomerization barrier. If, based on reported rate coefficients for $R^{\bullet}$+O_2 (Atkinson et al., 2006), one reaction among ten is assumed to be reactive, peroxyradicals are likely to be formed before the isomers are cooled below the isomerization barrier. Therefore, the equilibrium may be shifted if the reaction of the *trans* radical with O_2 is faster than the reaction of the *cis* radical. Measurements made with reduced partial pressure of O_2 could test this hypothesis. The *cis* and *trans* forms can also be interconverted latter in the photooxidation by the δ_1^5 isomerization. Therefore the observed discrepancy may also be attributed to the additional stability of the *cis* β-hydroxy allyl radical provided by the interaction between the alcohol groups.

Evidence for Dibble's mechanism. Both HACET (Fig. 7) and GLYC (Fig. 3) exhibit a very prompt source. To our knowledge, the mechanism proposed by Dibble (2004a,b) and reproduced in Sect. 4.1.1 is the only mechanism able to yield both compounds after a single OH reaction. For GLYC, we set the branching ratio quenching:thermalization to 7:3 in good agreement with the theoretical estimate (Dibble, 2004b). The same branching ratio was applied to capture the prompt formation of HACET from the $Z_{4,1}$ branch. Theoretical considerations do not support such a large hydroxyacetone formation (Dibble, 2004b). The hydroxyacetone rate constant with OH is set to k_{OH}=5.98×10^{-12} cm^3 molecule^{-1} s^{-1} (Dillon et al., 2006) and the rate constant of glycolaldehyde with OH is set to k_{OH}=8×10^{-12} cm^3 molecule^{-1} s^{-1} (Karunanandan et al., 2007).

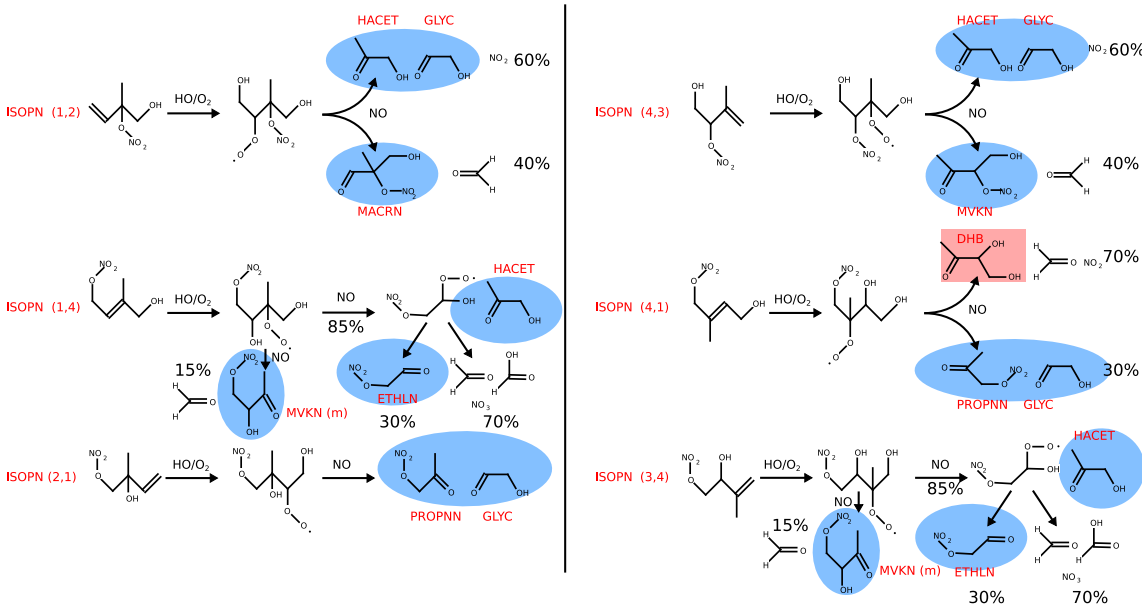

Fig. 8. Decomposition pathway of the different isoprene nitrates after their reaction with OH. Reaction of ISOPN with OH, O_2, and NO, also yields dihydroxy-dinitrates through Reaction (R7). Color code is identical to Fig. 1.

HC5 chemistry. HC5 (Fig. 2) exhibits a very fast decay consistent with a reaction rate coefficient with OH similar to isoprene ($1.0-1.2\times10^{-10}$ cm^3 molecule^{-1} s^{-1}). This estimate is consistent with the fastest rate recently derived by Baker et al. (2005) and ~80% greater than the SAR estimate (k_{OH}^{SAR}=6.82×10^{-11} cm^3 molecule^{-1} s^{-1} or 7.9×10^{-11} cm^3 molecule^{-1} s^{-1} with the correction from Bethel et al., 2001; Papagni et al., 2001) . This discrepancy can be partly explained by the effect of the alcohol group α of the double bond which enhances the addition of OH (Papagni et al., 2001). The large measured yield of MOBA=MOBA Z(1, 4)+MOBA Z(4,1) (Fig. 5) also suggests that the abstraction of the aldehydic hydrogen (channel ④) is faster than predicted, possibly related to a long distance interaction between the alcohol group and the carbonyl group (Neeb, 2000).

Experimental evidence for the formation of 3-methylfuran (3-MF) from the $Z_{1,4}$ and $Z_{4,1}$ branches have been reported (Tuazon and Atkinson, 1990). However the mechanism remains unclear with evidence for both heterogeneous formation (Baker et al., 2005; Dibble, 2007; Atkinson et al., 2008) from HC5 and homogeneous formation from its parent alkoxy (Francisco-Marquez et al., 2005).

In our model, 3-MF yield is set to 4.5% based on experimental results (Atkinson et al., 1989; Paulson et al., 1992) and formed from the parent alkoxy of HC5. As a result, 37% of the alkoxyradical formed in the $Z_{1,4}$ and $Z_{4,1}$ branches must decompose to 3-MF in order to match the experimental yield. We can not rule out 3-MF heterogeneous formation. We note, however, that if heterogeneous processes yield 3-MF, the calculated HC5 yield would be ~20% higher. Moreover, the decay rate required to match HC5 profile would likely be faster than observed. 3-MF formation mechanism has little impact on the conclusions of this paper but has significant consequences for atmospheric chemistry. Indeed if formed through heterogeneous processes, 3-MF yield is likely to be smaller than determined in atmospheric chambers. Further work is clearly required to quantify this issue and determine the products of 3-MF photooxidation.

We note, finally, that the observation of large yields for HC5 and 3-MF are consistent with an asymmetry between the E and Z branches. If the branching ratio E:Z were close to 1:1, the fraction of peroxy radical $Z_{1,4}$ and $Z_{4,1}$ required to decompose to 3-MF would be 62% and the yield of HC5 only 6.1% This is inconsistent with the yields previously reported (Baker et al., 2005).

4.2 Organic nitrates

The observation of the organic nitrates of isoprene and MVK/MACR as well as some of the products of their photooxidation (Figs. 8 to 13), provides constraints on the isoprene nitrate yields, their lifetimes and the amount of NO_x recycled through the first stage of their photooxidation as well as their lifetimes.

4.2.1 δ-hydroxy isoprene nitrates

The fate of the δ-hydroxy isoprene nitrates (1, 4) and (4, 1), respectively ISOPN (1, 4) and ISOPN (4, 1), can be followed through their degradation products (Fig. 8): ethanal nitrate (ETHLN) monitored at m/z=190 (Fig. 10) and propanone nitrate (PROPNN) at m/z=204 (Fig. 11).

PROPNN features a very prompt source, which requires a fast reaction rate coefficient of ISOPN(4, 1) with OH: $k_{OH}^{ISOPN(4,1)}$=9.5×10^{-11} cm^3 molecule^{-1} s^{-1}. This is ~45% faster than SAR and suggests an inadequate parameterization of the effects of nitroxy groups on the reactivity of the double bond (Neeb, 2000). No significant signal is observed at

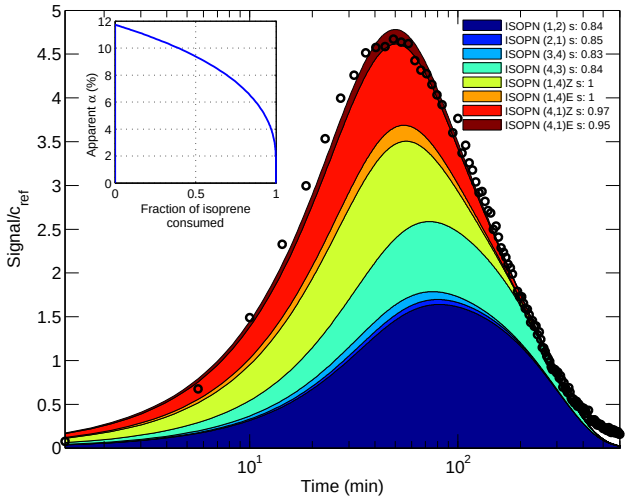

Fig. 9. Signal recorded at m/z=232 (black circles) compared to modeled isoprene nitrates (ISOPN (1, 2), (1, 4)E/Z, (2, 1), (4, 3), (3, 4), (4, 1)E/Z (measured as clusters)) corrected for calibration changes.

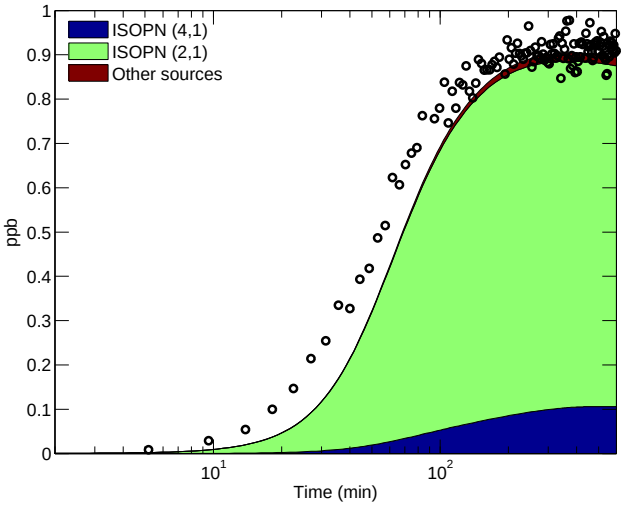

Fig. 11. Signal recorded at m/z=204 (black circles) compared to modeled PROPNN (measured as a cluster). Colored bars indicate the instantaneous modeled contributions of the different sources of PROPNN.

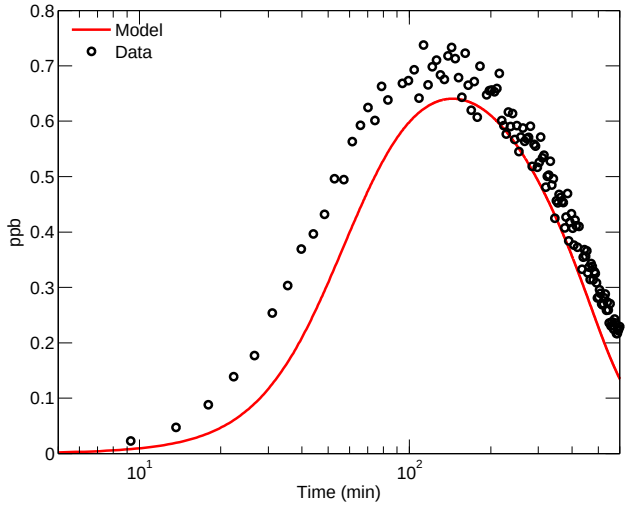

Fig. 10. Signal recorded at m/z=190 (black circles) compared to modeled ETHLN (measured as a cluster).

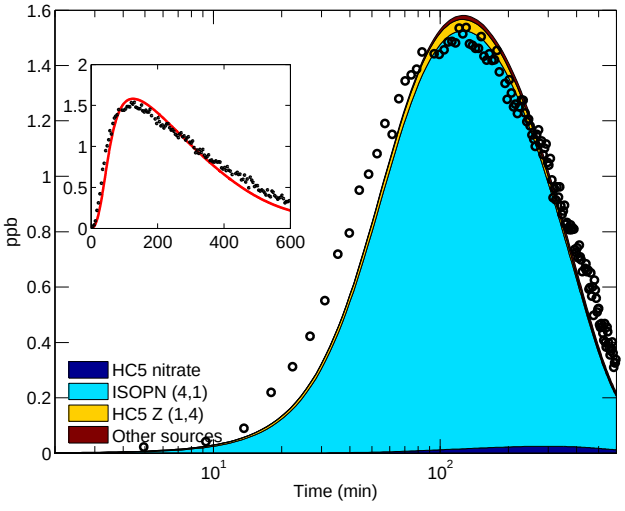

Fig. 12. Signal recorded at m/z=189 (black circles) compared to modeled DHB (measured as a cluster). Colored bars indicate the instantaneous modeled contributions of the different sources of DHB.

m/z=230, confirming that the abstraction of the hydrogen in α of the alcohol of ISOPN is negligible compared to addition on the double bond.

SAR suggests that ISOPN(1, 4) and ISOPN(4, 1) are similarly short-lived with respect to OH. This is consistent with the prompt source of ETHLN (Fig. 10), a product of the oxidation of ISOPN (1, 4) (Fig. 8). The use of the primary nitrate photolysis rate (cf. A3) and SAR rate estimate for the reaction ETHLN + OH underpredicts its decay. To match the measured profile (Fig. 10), we take k_{OH}=1×10^{-11} cm^3 molecule^{-1} s^{-1} , three times faster than the SAR estimate. If the ETHNL photolysis rate is larger than estimated (J$\sim4\times10^{-7}$ s^{-1} using 1$-$C$_4$H$_9$ONO$_2$), ETHLN reaction rate coefficient with OH would be commensurately slower.

NO_x recycling from the (4, 1) branch is $\sim$70% based on the measured ratio PROPNN: dihydroxybutanone (DHB, cluster at m/z=189). The reaction rate coefficient of DHB with OH is estimated to be 1.3×10^{-11} cm^3 molecule^{-1} s^{-1} or 60% of SAR (Fig. 12).

The yield of ETHLN is substantially overestimated if the yield of the reaction RC$^{\cdot}$OH + O_2 $\rightarrow$ RCO + HO_2 is 100%. As will be discussed further in Sect. 4.3, we suggest that

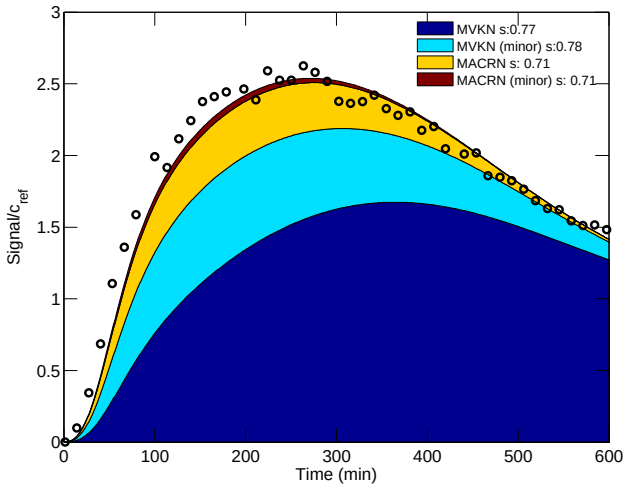

Fig. 13. Signal recorded at m/z=234 (black circles) compared to the modeled profile of MVKN+MVKN (m)+MACRN+MACRN (m) (measured as clusters) corrected for changing calibrations.

unimolecular decomposition of the α-hydroxyperoxy radical from ISOPN(1, 4) yields formic acid, resolving this discrepancy.

4.2.2 β-hydroxy isoprene nitrates

To capture the decay of the m/z=232 signal requires that β-hydroxy isoprene nitrates (ISOPN (1, 2), (2, 1), (4, 3) and (3, 4)) be much longer-lived than δ-hydroxy isoprene nitrates (ISOPN (1, 4) and (4, 1)). Unfortunately, the products of their photooxidation have multiple other sources, precluding a direct derivation of their lifetime. For instance methylvinylketone nitrate (MVKN) and methacrolein nitrate (MACRN) are also formed from MVK and MACR with similar rates. The evolution of the m/z=232 signal can be captured when the SAR chemical rates for these nitrates are reduced by 20%.

The reaction of the isoprene nitrate with ozone is included for ISOPN (1, 2) and ISOPN (4, 3), because their long lifetimes allow them to encounter high concentrations of ozone in the chamber (Fig. A2). We do not observe the formation of 3 hydroxy-2-nitrooxy-2-methyl propanoic acid (no correlation between m/z=184 and m/z=250). Therefore, we use a simplified version of the ozonolysis products proposed by Giacopelli et al. (2005) assuming that this reaction yields only MACRN and MVKN. These reactions contribute significantly to the total yield of MVKN and MACRN in this experiment.

4.2.3 Methacrolein and methylvinylketone hydroxynitrates

MVKN and MACRN are monitored through their clusters with CF_3O^- at m/z=234 (Fig. 13).

MACRN features an aldehyde group which suggests a much faster decomposition than MVKN. This is confirmed by the profile of hydroxyacetone which does not exhibit any significant late source. As a result, the third regime of the experiment is dominated by MVKN and its reaction rate coefficient with OH can be estimated: k_{OH}^{MVKN}=2.8×10^{-12} cm^3 molecule^{-1} s^{-1}. The yield of MVKN can be constrained using GLYC profile since MVK is its major source: α_{MVK}=(11±3)%. Applying the same approach to MACR/MACRN/HACET is more complicated since hydroxyacetone has many more sources than glycolaldehyde (Fig. 7). We find that a yield of MACRN of (15±3)% and a reaction rate coefficient with OH of 5×10^{-11} cm^3 molecule^{-1} s^{-1} best match the peak time of m/z=234. These values are consistent with the study of Chuong and Stevens (2004).

The abstraction of the hydrogen α to the alcohol in MACRN, MVKN and MVKN (m) is expected to yield dicarbonyl nitrates. We expect CIMS to be sensitive to this class of compounds since we are able to measure compounds featuring a carbonyl in β of the nitrate group, such as PROPNN or ETHLN. Since m/z=232 only features early stages compounds, isoprene nitrates, there is no evidence for the formation of dicarbonyl nitrates. Recent theoretical studies (Peeters et al., 2001; Hermans et al., 2005) show that primary α-hydroxy-alkylperoxy radicals can be sufficiently stabilized to undergo reactions with NO and yield formic acid. Nevertheless the photooxidation of MVKN occurs in a mostly low-NO_x environment which suggests that α-hydroxy-alkylperoxy radicals may undergo an intramolecular decomposition to yield a carboxilic acid and the nitrate radical. Such a reaction may involve a four or six-e$^-$ mechanism.

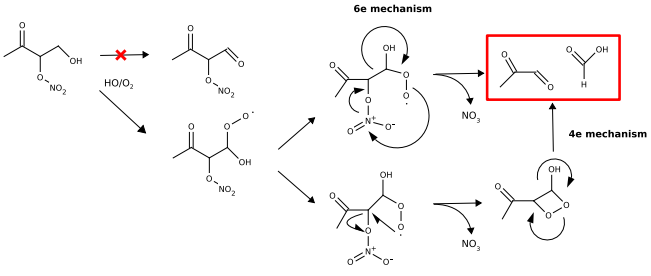

Finally, m/z=234 signal features a prompt source which can not be accounted for by MVK or MACR nor by the β-hydroxy isoprene nitrates, which have a similar lifetime with respect to OH. Conversely ISOPN (1, 4) is very short-lived and a MVKN (m) yield of 10–15% enables to capture this feature (Fig. 13).

4.3 Acids

4.3.1 Formic acid

Formic acid is detected as a cluster (m/z=131) and a transfer (m/z=65) with about equal sensitivity. At the NO_x titration

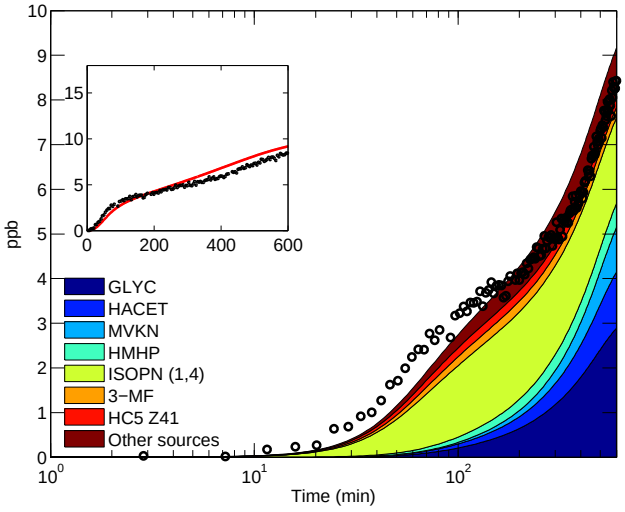

Fig. 14. Signal recorded at m/z=65 (black circles) compared to modeled formic acid. Colored bars indicate the instantaneous modeled contributions of the different sources of formic acid.

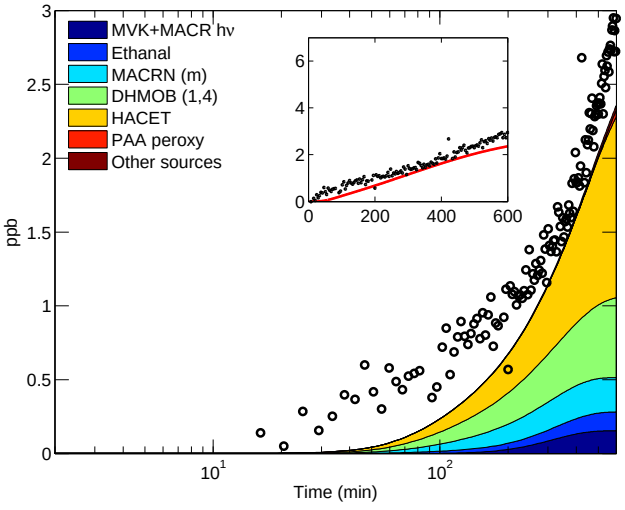

Fig. 15. Signal recorded at m/z=79 (black circles) compared to modeled acetic acid (observed as a transfer at this mass). Colored bars indicate the instantaneous modeled contributions of the different sources of acetic acid.

(∼600 min), a molar yield of about (10±3)% is obtained (Fig. 14).

The measured profile of formic acid (Fig. 14) features the three characteristic chemical regimes of this experiment as described (cf. Sect. 3).

First regime. A very early source of formic acid is noticeable (Fig. 14). Several observations suggest that formic acid may be formed from an intramolecular decomposition of ISOPN (1, 4) similar to the one described for MVKN earlier: 1) This source is absent from the experiments performed in the absence of NO_x 2) the early formic acid profile correlates very well with the propanone nitrate which originates from ISOPN (4, 1) decomposition 3) ETHNL would be largely overevaluated in the absence of other decomposition channel for ISOPN (1, 4). Matching the ETHLN profile (Fig. 10) results in a branching ratio for formic acid to ETHLN of 3:1. ISOPN(2, 1) may yield acetic acid, but is not included since its contribution would be negligible.

Bierbach et al. (1995) report 4-oxo-pentenal as the major product of the photooxidation of 2-methylfuran in the absence of NO_x, while formic acid accounts for about 6%. We are unaware of any study of the photooxidation of 3-MF in the presence of NO_x. Since the reaction rate coefficient of methylfuran with OH is similar to that derived for ISOPN (1, 4) and (4, 1), its photooxidation may contribute to the early sources of formic acid:

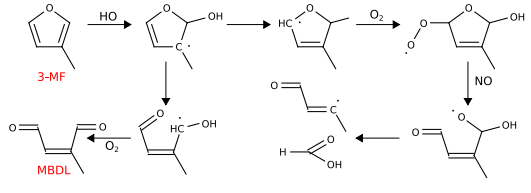

Second regime. Butkovskaya et al. (2006a,b) report a formic acid yield from the photooxidation of GLYC (HAC) of 18% (respectively 7%). The formation of formic acid from the decomposition of MVKN described in Sect. 4.2.3 also plays a minor role in this regime.

Third regime (not shown). As NO_x becomes limiting, hydroxymethyl hydroperoxide (HMHP) formation from the reaction of CH_2OO with water is enhanced. HMHP can account for most of the late formation of formic acid through its reaction with OH and its photolysis. A large additional source is missing, however, in the mechanism. Heterogeneous decomposition of HMHP (Neeb et al., 1997) and aerosol processes (Walser et al., 2007) are likely to account for this missing source. An upper limit for the strength of the aerosol source can be estimated from the decrease of the aerosol volume $-2.5\,\mu m^3/cm^3$ which would represent a release of 2.6 ppbv C=O in the chamber assuming a density of $1.25\,g/cm^3$ (Kroll et al., 2006). Since the same phenomenon is observed for acetic acid (Fig. 15), most likely both HO_x-dominated VOC oxidation as well as organic aerosol oxidation are needed to explain the observed increase in formic and acetic acid in the third regime.

4.3.2 Acetic acid

The production of acetic acid (Fig. 15) occurs primarily through the oxidation of hydroxyacetone as described by Butkovskaya et al. (2006b). Additional routes include direct formation from $CH_3CHO + OH$ (Cameron et al., 2002) as well as $CH_3C(O)OO + HO_2$ following Reaction (R11).

Two additional minor routes are hypothesized: 1) decomposition of MACRN(m), 2) decomposition of DHMOB (1, 4) (m/z=217), inspired by the mechanism proposed by Butkovskaya et al. (2006a). Following their analysis, we assume a 37% acetic molar yield, the remaining falling apart as CO_2 and hydroxybutane-2,3-dione (m/z=187).

Table 2. Isoprene nitrate kinetic data. The uncertainty is smaller than 30%.

	Molar yield %	α %	k_{OH} $\times 10^{-11}$	k_{O_3} $\times 10^{-17}$	Recycling (cf. text)
ISOPN 1,2	2.7	6.7	1	1	45
ISOPN 1,4 Z	3.1	24	9.5		52
ISOPN 1,4 E	0.54	24	9.5		52
ISOPN 2,1	0.13	6.7	3.4		-10
ISOPN 3,4	0.33	6.7	6.6		52
ISOPN 4,3	1.5	6.7	1.9	1	56
ISOPN 4,1 Z	2.9	24	9.5		68
ISOPN 4,1 E	0.51	24	9.5		68
Weighted Average	11.7				55

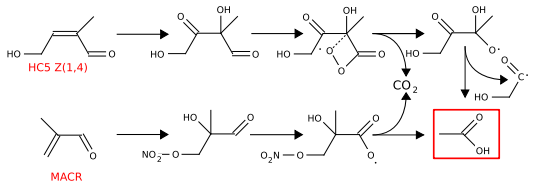

4.3.3 MOBA

MOBA, the class of five-carbon acids identified at m/z=133 and 199 in Sect 4.1 can react with OH and ozone under the chamber conditions. The slow decay of the signal suggests that its reactivity is dominated by ozone in the chamber and that the acid group significantly hinders the addition of OH onto the double bond. A good match is obtained by setting k_{OH} equal to 3×10^{-12} cm^3 molecule^{-1} s^{-1} (F_{COOH}=0.1 in terms of SAR) and k_{O_3}=2×10^{-17} cm^3 molecule^{-1} s^{-1}.

Little signal is observed at m/z=93 which suggests no or minor formation of oxoacetic acid. This suggests that the reaction with OH does not conserve the acid group, which is likely lost as CO_2. Pyruvic acid can be expected to be a major product of MOBA ozonolysis.

4.3.4 Pyruvic acid

Pyruvic acid is a precursor for glyoxylic and oxalic acids, two carboxylic acids detected in the aerosol phase (Carlton et al., 2006). It is observed as a cluster at m/z=173 in association with HOPL, a product of DHPL photooxidation. Due to its stickiness to the walls of the flow tube, the theoretical calibration is expected to largely overestimate our sensitivity to this compound. The yield of pyruvic acid after 600 min is 2±1%.

Qualitatively, the major sources of pyruvic acid are expected to include (heterogeneous) hydrolysis of the Criegee intermediate produced in the ozonolysis of MVK and MOBA as well as the decomposition of MVKN(m) following the scheme presented in Sect. 4.2.3.

4.4 Atmospheric relevance

4.4.1 Fate of organic nitrogen

The formation of organic nitrates, and more specifically isoprene nitrates, play an important role in determining the amount of NO_x and thus ozone production in many environments.

The observation of isoprene nitrate clusters with CF_3O^- as well as some of the products of their photooxidation, provides constraints on the isoprene nitrate yields, the amount of NO_x recycled through the first stage of their photooxidation, and their lifetimes (Table 2). These three parameters are necessary to accurately assess the influence of isoprene photooxidation on atmospheric chemistry.

Yield. Previous estimates for the isoprene nitrate yield, α, span a very large range. Chen et al. (1998) reported an overall yield of 4.4%, Chuong and Stevens (2002), 15% using an indirect method, Sprengnether et al. (2002), 12%, Patchen et al. (2007), 7% at 130 hPa. Using experimental yields collected for compounds similar to isoprene, Giacopelli et al. (2005) estimated the nitrate yield of the β and δ-hydroxy isoprene nitrates to be respectively 5.5% for the former and 15% for the latter, for an overall yield of 8.6%. Since organic nitrates sequester NO_x, such a large variation in the estimated yields has profound implications to the assessments of ozone production caused by isoprene photooxidation (von Kuhlmann et al., 2004; Fiore et al., 2005; Horowitz et al., 2007).

We report a yield of (11.7±3)% with a large discrepancy between the yields of the nitrates originating from δ ($\simeq$24%) and β-hydroxy channels ($\simeq$6.7%). We emphasize, however, that we derived a total yield rather than specific branching ratios so that the specific organic nitrate yields are affected by the choice of the initial β:δ-hydroxy channel ratio (cf. Sect. C1). Nevertheless, the discrepancy between δ-hydroxy channels and β-hydroxy channels is a reliable feature, with the δ-hydroxy isoprene nitrates accounting for about 60% of the total isoprene nitrate yield. Giacopelli et al. (2005) suggested this behaviour previously using measurement collected for similar compounds.

Lifetime. The efficiency of both NO_x transport and removal through organic nitrates is related to their lifetimes. The transport of isoprene-nitrates and their alkylnitrate degradation products is of special importance since it is thought to be a major source of NO_x in rural areas (Horowitz et al., 1998). In this NO_x-limited environment, the release of NO_x through their decomposition would greatly influence O_3 production. In the absence of experimental data, Giacopelli et al. (2005) estimated using Kwok's SAR that the δ-hydroxy isoprene nitrates should be significantly shorter-lived than the β-hydroxy isoprene nitrates. With the help of the propanone nitrate profile, we can experimentally confirm this discrepancy (Table 2). With [OH] =10^6 molecule^{-1} cm^{-3}, the photochemical lifetime with OH of the δ-hydroxy isoprene nitrates (respectively the β-hydroxy isoprene nitrate) is τ^{δ}_{OH}=3 h (τ^{β}_{OH}=18 h). Horowitz et al. (2007) show that the deposition of isoprene nitrates is likely to be dominated by dry processes and that $\tau_d^{HNO_3}\simeq 7\,h \leq \tau_d^{ISOPN} \leq \tau_d^{PAN}\simeq 100\,h$. As a result, the fate of the δ-hydroxy isoprene nitrates is likely to be dominated by their reactivity with OH and possibly O_3 similar to isoprene while other

processes such as dry deposition and reaction with NO_3 must be taken into account for proper modeling of the β-hydroxy isoprene nitrates. Therefore, the latter are likely to have greater influence on tropospheric chemistry.

The large difference in the lifetime of the organic nitrates formed in the δ-hydroxy and β-hydroxy channels may explain some of the spread in the reported yields and NO_x recyclings. Studies focusing on the very first step of isoprene photooxidation (e.g. Sprengnether et al., 2002) tend to report the highest nitrate yield, suggesting that the short-lived δ-hydroxy isoprene nitrates may have been underestimated in some previous experiments (see inset of Fig. 9). The same argument may also explain the observations of a greater variety of isoprene nitrates in laboratory experiments than in the field (Giacopelli et al., 2005).

Recycling. The efficiency of the NO_x sequestration depends on the fate of the isoprene nitrates and more specifically on how much NO_x is released in their subsequent photooxidation. NO_x-recycling is defined as the difference between the NO_x released by the reaction and the NO consumed. As a result, since ISOPN(2, 1) oxidation does not yield any NO_2, its recycling is negative due to the formation of dinitrates (Fig. 8 and Table 2), which we have observed at m/z=311 in another experiment. Horowitz et al. (2007) obtain the best agreement with the boundary layer data when 40% of the NO_x is recycled with a low nitrate yield (4%). We find a NO_x recycling of (55%±10)% by the isoprene peroxy radicals consistent with Horowitz et al. (2007) conclusion despite our very different yields. As highlighted in the inset of (Fig. 9), this may be related to the wrong estimation of isoprene nitrate yield due to the short lifetime of the δ-hydroxy channels.

The photooxidation of isoprene leads to the formation of other significant organic nitrates MVKN, MACRN, PROPNN (≃1%) and ETHLN (≃1%). All these compounds are substantially longer-lived than isoprene nitrates and therefore are more likely to influence the NO_x-balance on a larger scale (assuming a similar deposition velocity). The formation of PROPNN and MVKN appear especially important as their photochemical sinks are very slow: $\tau_{OH}^{MVKN} \simeq 100\,h$ and $\tau_{OH}^{PROPNN} > 200\,h$. Therefore, they may constitute important pathways for NO_x transport as well as significant NO_x-sinks through deposition. They also can contribute to the growing source of atmospheric nitrogen to the open ocean (Duce et al., 2008).

In contrast to ISOPN, MACRN and MVKN release most of their NO_x in the course of their decomposition, possibly through the formation of formic and pyruvic acids. These organic nitrate channels may contribute significantly to the missing source of small carboxylic acid in the free troposphere.

4.4.2 Acids

Small carboxilic acids are ubiquitous in the atmosphere both in the gas-phase and in the aqueous phase, playing an important role in rain acidity and cloud reactions (Chebbi and Carlier, 1996).

The photooxidation of isoprene under high NO_x produces substantial amounts of formic (yield ≃(10±3)% after 600 min) and acetic acids (yield ≃(3±1)% after 600 min). Acetic and formic acids are highly correlated after the first 150 minutes (ρ=0.988), since their main source, hydroxyacetone for acetic acid and glycolaldehyde for formic acid, share a similar origin and lifetimes (Figs. 14 and 15). We find [Acetic Acid]=0.46±0.02 × [Formic Acid]−0.02 ± 0.01 × $[\text{Isoprene}]_0$.

A strong correlation between formic and acetic acids has been observed previously over Amazonia (Andreae et al., 1988) and Virginia (Talbot et al., 1995). In most large scale chemical models, these compounds originate primarily from biomass burning and to a lesser extent from ozonolysis of alkenes. Since the main source of both acids in the chamber is unlikely to result from the ozonolysis of the alkenes, our study shows that additional channels for their formation should be included. The main identified sources (hydroxyacetone, glycolaldehyde, organic nitrates) are much longer-lived than the ones currently included in global model which may help resolve part of the discrepancy between models (Jacob and Wofsy, 1988) and atmospheric observations (Andreae et al., 1988; Talbot et al., 1990).

Finally the identification of MOBA, a five carbon acid, could be important for aerosols as its vapor pressure and the vapor pressures of the products of its photooxidation are expected to be low.

4.4.3 Development of a reduced mechanism

The new constraints derived in this study primarly originate from our observation of the chemistry of the δ-hydroxy channels. In particular, we have shown that these channels account for a large fraction of the isoprene nitrates and small carboxylic acids, whose role is important on a global scale. Most of the reduced isoprene photooxidation mechanism implemented in chemical transport models, e.g. MOZART (Pfister et al., 2008), do not adequatly account for the chemistry of the δ-hydroxy channels, thus impeding proper modeling of the consequences of isoprene photooxidation on troposheric chemistry.

The detailed chemical mechanism described in this study is too complex to be included in large scale atmospheric chemistry simulations. To aid in such investigations, we propose that a few modifications of these simplified mechanisms be implemented (Table 3). While adding little complexity and maintaining carbon balance, these few changes describe more accurately the formation and fate of nitrates as well as the yield of carboxylic acid. In particular, the long life time of PROPNN and MVKN enables transport of organic nitrates over long distances.

In our reduced mechanism, we neglect the E δ-hydroxy channel branch (≃5% of the carbon) as well as the non-Dibble branch yielding MPDL and OBL (Fig. 1). We have only included the formation of organic nitrates which

Table 3. Suggested modifications of isoprene condensed photooxidation mechanism under high NO_X conditions. (2, 1), (3, 4), E(1, 4) and E(4, 1) branches are not treated. Formation of organic nitrates is limited to isoprene, MVK and MACR peroxy radicals. The reaction of the isoprene nitrates with respect to O_3 as well as the fate of 3-MF are not tackled by this mechanism (cf. text). MGLYX denotes methylglyoxal and HC4, a generic four-carbon VOC.

Reaction			k (T=298 K) 10^{-11}cm^3 molecule^{-1} s^{-1}
ISOP + OH	→	$ISOPO_2$	10
$ISOPO_2$ + NO	→	0.40 MVK + 0.26 MACR + 0.883 NO_2 + 0.07 $ISOPN_\delta$ + 0.047 $ISOPN_\beta$ + 0.66 HCHO 0.10 HC5 + 0.043 (3−MF) + 0.08 DIBOO + 0.803 HO_2	0.81
HC5 + OH	→	HC5OO	11
HC5OO + NO	→	NO_2 + 0.234 (GLYC + MGLYX) + 0.216(GLYX + HACET) + 0.29 DHMOB 0.17 MOBA + 0.09 HC4 + 0.09 CO + HO_2	0.81
$ISOPN_\delta$ + OH	→	$ISOPNOO_\delta$	9.5
$ISOPNOO_\delta$ + NO	→	0.34 DHBN + 0.15 PROPNN + 0.44 HACET + 0.07 MVKN + 0.13 ETHLN + 0.31 HCOOH + 0.31 NO_3 +0.72 HCHO + 0.15 GLYC + 1.34 NO_2 + 0.35 HO_2	0.81
$ISOPN_\beta$ + OH	→	$ISOPNOO_\beta$	1.3
$ISOPNOO_\beta$ + NO	→	0.6 (GLYC + HACET) + 0.4 (HCHO + HO_2) + 0.26 MACRN + 0.14 MVKN + 1.6NO_2	0.81
DIBOO + NO	→	NO_2 + HO_2 + 0.52(GLYC + MGLYX) + 0.48(GLYX + HACET)	0.81
MVK + OH	→	MVKOO	1.75
MVKOO + NO	→	0.625 (GLYC + $CH_3C(O)OO$) + 0.265 (MGLYX + CH_2O + HO_2) + 0.11 MVKN 0.89 NO_2	0.81 0.81
MVKN + OH	→	0.65 (HCOOH + MGLYX) + 0.35 (CH_2O + $CH_3C(O)C(O)OH$) + NO_3	0.56
MACR + OH	→	0.47 MACROO + 0.53 MCO_3	2.95
MACROO + NO	→	0.85 (NO_2 + HO_2) + 0.425 (HACET + CO) + 0.425 (CH_2O + MGLYX) + 0.15 MACRN	0.81
MACRN + OH	→	0.08 ($CH_3C(O)OH$ + CH_2O + NO_3) + 0.07 (HCOOH + NO_3 + MGLYX) 0.85 (HACET + NO_2) + 0.93 CO_2	5
MC(O)OO + NO	→	NO_2 + CO + CO_2 + CH_2O + CH_3OO	2.1
GLYC + OH	→	0.75 HO_2 + 0.25 OH + 0.13 GLYX + 0.52 CO + 0.35 CO_2 + 0.16 HCOOH + 0.71CH_2O	0.8
HACET + OH	→	0.75 MGLYX + 0.825 HO_2 + 0.125 HCOOH + 0.1 OH + 0.125 CH_3OO + 0.20 CO_2 0.05 CO + 0.125 $CH_3C(O)OH$	0.6
ETHLN + OH	→	CH_2O + CO_2 + NO_2	1
DHMOB + OH	→	1.5 CO + 0.5 HO_2 + 0.5 HACET + 0.5 HC4	1
MOBA + HO	→	MOBAOO	0.3
MOBAOO + NO	→	HC4 + CO_2 + HO_2 + NO_2	0.8

were directly constrained in this study (ISOPN, PROPNN, ETHNL). The yield of minor organic nitrates can be derived using the number of carbons of the parent peroxy radical, a common approach in most chemical transport models. We introduce a generic four carbon hydrocarbon, HC4, to account for the decomposition of MOBA. This study does not constrain the fate of 3-methylfuran and the reaction of isoprene nitrates with ozone; more theoretical and experimental work is required.

5 Conclusions

A substantial fraction of the terrestrial Northern Hemisphere is characterized by conditions in which the fate of isoprene peroxy radicals is dominated by reactions with NO. Chameides et al. (1988) demonstrated that they play a major role in the formation of ozone in urban areas. This study complements previous investigations of isoprene photooxidation mechanism by focusing on the δ-hydroxy channels, whose chemistry is not adequately represented in chemical transport models. We focus on the large yields of small carboxylic acids and propose new constraints for the yield and the fate of organic nitrates. Both constitute outstanding uncertainties in the photooxidation of isoprene, impeding proper modeling of tropospheric chemistry on a global scale. To aid in the development of improved simulations of this chemistry, we propose simple modifications of current condensed mechanism which maintains carbon balance and accounts for the new constraints and mechanisms identified in this study (Table 3).

Appendix A

Photooxidation mechanism

A1 VOC chemistry

Except as noted below, we use the known rate coefficients of bimolecular and termolecular reactions as tabulated in IUPAC (Atkinson et al., 2004, 2006) and JPL (Sander, 2006) reports.

A1.1 HO

Reactions of HO with VOC are limited to its addition on a double bond and the abstraction of the aldehydic hydrogen and the hydrogen in α to an alcohol, i.e. the abstraction of hydrogens from alcohols is neglected. For the addition of HO onto double bonds, in the absence of data or previous

information enabling differentiation between the two carbons, we assume that the reaction occurs only on the most favorable location based on steric considerations. A structure-activity relationship (SAR) method is used to determine unknown reaction rate coefficients (Kwok and Atkinson, 1995).

Following the studies of Orlando and Tyndall (2001) and Méreau et al. (2001), acylradicals are assumed to decompose promptly when the alkyl group features a carbonyl or an alcohol (with R secondary or tertiary) in β to the carbonyl:

$$R_1R_2R_3CCHO + HO \rightarrow R_1R_2R_3CCO + H_2O \quad (R5)$$

$$R_1R_2R_3CCO \rightarrow R_1R_2R_3C + CO \quad (R6)$$

We also assume that acylradicals featuring a nitrooxy group in β to the carbonyl undergo unimolecular decomposition. In all other cases, the acyl radical is assumed to add O_2 to yield the associated peroxy radical.

In case of resonance, the branching between the addition of O_2 on the carbon in α of alcohol (denoted ⓐ in Fig. 1) or in γ (ⓑ) is unknown. Addition on ⓐ features a more stable double bond as well as a kinetically favored radical. In the mechanism, we set the branching ⓐ:ⓑ to 65%:35%. Furthermore we note that HOPL does not exhibit any early source, suggesting that the yield of HMPL is negligible. Indeed, its formation appears unfavorable on both a thermodynamic (the double bond is less substituted) and a kinetic (formation of a secondary radical) basis. Thus, the branching ratio is set to $Y_a^{E_{(1,4)}}$=95% and $Y_b^{E_{(1,4)}}$=5%.

A1.2 Ozone

Ozone reacts with alkenes via the formation of a molozonide, quickly followed by its decomposition into a carbonyl and a Criegee intermediate. Assuming a generic rate constant for the reaction of alkenes with ozone, 10^{-17} $cm^3\,molecule^{-1}\,s^{-1}$, the reaction of an alkene with ozone is included if $\tau_{HO} > \frac{\tau_{O_3}}{10}$, where τ_{HO} and τ_{O_3} are the lifetimes of the alkenes with respect to HO and O_3 respectively.

Ozone reactions are included for isoprene, MACR and MVK, following IUPAC recommendations.

A1.3 NO_3

Reactions of NO_3 with alkenes and aldehydes have been neglected, since $\frac{k^{NO_3}_{\{alkenes/aldehydes\}}[NO_3]}{k^{HO}_{\{alkenes/aldehydes\}}[HO]} \ll 1$ throughout the experiment.

A2 Peroxyradical chemistry

A2.1 NO

NO reacts with peroxy radicals with a rate coefficient of $2.43\times10^{-12}\exp(360/T)$ $cm^3\,molecule^{-1}\,s^{-1}$ (Atkinson et al., 2006) through

$$RO_2 + NO \rightarrow (1-\alpha)(RO + NO_2) + \alpha RONO_2 \quad (R7)$$

The reaction rate coefficient of acyl peroxy radical with NO is set to $6.7\times10^{-12}\exp(340/T)$ $cm^3\,molecule^{-1}\,s^{-1}$ based on $CH_3CH_2C(O)OO$.

Carter's parameterization is used to compute the alkyl nitrate yield (Carter and Atkinson, 1989; Arey et al., 2001):

$$\frac{\alpha}{1-\alpha} = \frac{Y_0^{298}[M](T/298)^{-m_0}}{1+\Theta} F^Z \times m \quad (A1)$$

with $z=(1+[\log(\frac{Y_o^{298}[M](T/298)^{-m_0}}{Y_\infty^{298}[M](T/298)^{-m_\infty}})]^2)^{-1}$, F=0.41, m_0=0, m_∞=8.0, β=1, $\Theta=\frac{Y_0^{298}[M](T/298)^{-m_0}}{Y_\infty^{298}(T/298)^{-m_\infty}}$, $\gamma=2\times10^{-22}$ $cm^3 molecule^{-1}$, Y_∞^{298}=0.43, $Y_0^{298}=\gamma e^{\beta n}$, where n is the number of carbons in the molecule. The parameter m is set to 0.4, 1.0 and 0.3 for primary, secondary and tertiary nitrates, respectively (Arey et al., 2001).

For β-hydroxy peroxy radicals, α is divided by two to account for the effect of the hydroxy group as highlighted by O'Brien et al. (1998).

For acylnitrates, the yield is set to the alkyl tertiary nitrate yield, providing it does not exceed 4%.

A2.2 NO_2

NO_2 reacts with peroxy acyl radicals to yield peroxyacylnitrate-like compounds, which decompose thermally or photolytically:

$$RC(O)OO + NO_2 \leftrightarrows RC(O)OONO_2 \quad (R8)$$

The rates of formation and decomposition of methyl peroxyacylnitrates (MPAN) are used for all PAN-like compounds except PAN itself. Most PAN-like compounds except PAN itself have other reactive groups (aldehyde, primary or a secondary alcohol, double bond) causing their major sink to be reaction with HO.

A2.3 NO_3

NO_3 reacts with peroxy radicals through

$$NO_3 + RO_2 \rightarrow NO_2 + RO + O_2 \quad (R9)$$

The rate coefficient is set to 2.3×10^{-12} $cm^3\,molecule^{-1}\,s^{-1}$ independent of both the temperature and the peroxyradical.

A2.4 HO_2 and peroxy radicals

HO_2 reacts with peroxy radicals through four different channels:

$$HO_2 + RO_2 \rightarrow ROOH + O_2 \quad (R10)$$

$$\rightarrow ROH + O_3 \quad (R11)$$

$$\rightarrow RO + HO + O_2 \quad (R12)$$

$$\rightarrow R_{-H}O + H_2O + O_2 \quad (R13)$$

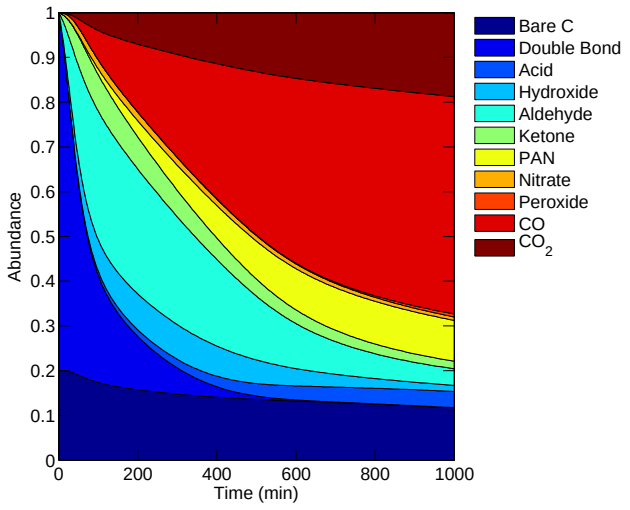

Fig. A1. Evolution of the speciation during isoprene photooxidation. The abundance of a functional group Π is defined as the sum of the carbons bearing Π normalized by the total amount of carbon in the chamber, i.e. five times the initial amount of isoprene.

Reaction (R13) has only been observed for compounds such as RCH_2OCH_2OO and is not considered in this study. Acyl peroxides are assumed to react through Reaction (R10), Reaction (R11) and Reaction (R12) with a branching ratio 0.4:0.2:0.4 (Hasson et al., 2004; Jenkin et al., 2007). Acetonylperoxy radicals have also been shown to react through channels Reaction (R10) and Reaction (R12) with a branching ratio 1:2 (Hasson et al., 2004). The other alkylperoxy are assumed to react through Reaction (R10) only.

The reaction rate coefficient for the reaction of alkylperoxy with HO_2 is set to $2.91\times10^{-13}\exp(1300/T)\times(1-\exp(-0.245n_c))$ $cm^3\,molecule^{-1}\,s^{-1}$ where n_c is the number of carbon atoms (Saunders et al., 2003). For the acyl peroxy radicals, the reaction rate coefficient is set to $5.2\times10^{-13}\exp(983/T)\,cm^3\,molecule^{-1}\,s^{-1}$ based on the reaction of the methylacylperoxy radical.

RO_2+RO_2 reactions are neglected in this study. In the early stages of isoprene photooxidation the chemistry of peroxyradicals is entirely dominated by NO. At the end of the experiment, peroxy radical chemistry is dominated by HO_2, which concentration is high enough so that RO_2 + RO_2 reactions can be safely neglected.

A3 Photolysis

The photolysis rate of a compound i is computed via:

$$J_i = \int_{\lambda_1}^{\lambda_2} \mathcal{I}^e(\lambda)\sigma_i\,(\lambda)\,\phi_i\,(\lambda)\,d\lambda \qquad \text{(A2)}$$

The effective light flux $\mathcal{I}^e$ is computed using an experimental determination of J_{HONO} and a spectrum of the lamp output made every nanometer (LI-COR LI1800 λ_1=300 nm, λ_2=600 nm). σ_{HONO} is scaled using the oscillator strength recently reported by Wall et al. (2006). This gives $J_{HOOH} = 3.1\times10^{-6}\,s^{-1}$.

The photolysis of compounds with unknown absorption cross sections is estimated from the known photolysis rate constants of similar compounds. The photolysis of organic nitrates is assumed to yield only $RO + NO_2$. For primary organic nitrate, the photolysis rate is taken from $1-C_4H_9ONO_2$, for secondary organic nitrates from $2-C_4H_9ONO_2$ and for tertiary nitrates from tertbutylnitrate (Roberts and Fajer, 1989; Atkinson et al., 2006).

A4 Fate of the alkoxy radicals

Alkoxy radicals can react following three different pathways:

$$R_1R_2R_3CO^{\cdot} \rightarrow R_1R_2CO + R_3^{\cdot} \qquad \text{(R14)}$$

$$+O_2 \rightarrow R_1R_2CO + HO_2 \text{ if } R_3 = H \qquad \text{(R15)}$$

$$\rightarrow R_1R_2COHCCCC^{\cdot}R'_3 \qquad \text{(R16)}$$

$$\text{with } R_3 = CCCCR'_3$$

Since the isomerization reaction, Reaction (R16), requires at least four carbons (Atkinson, 1997), it occurs only in the first stages of isoprene photooxidation, when major products retain five carbons. In the case of isoprene, isomerization (Reaction (R16)) is faster than decomposition (Reaction (R14)) and reaction with O_2 (Reaction (R15)). Alkoxy radicals which cannot undergo Reaction (R16) are assumed to decompose through Reaction (R14), i.e. their reaction with O_2 (Reaction (R15)) is generally neglected except for a few cases detailed in the discussion section.

Generally the decomposition of an alkoxy radical can occur through different channels, whose branching ratios (Y_i) are estimated using their respective activation energies, E_{bi}.

$$R_1R_2R_3CO^{\cdot} \rightarrow R_2R_3CO + R_1^{\cdot} \qquad \mathcal{Y}_1 \qquad \text{(R17)}$$

$$R_1R_2R_3CO^{\cdot} \rightarrow R_1R_3CO + R_2^{\cdot} \qquad \mathcal{Y}_2 \qquad \text{(R18)}$$

$$R_1R_2R_3CO^{\cdot} \rightarrow R_1R_2CO + R_3^{\cdot} \qquad \mathcal{Y}_3 \qquad \text{(R19)}$$

with

$$\forall i \in (1,2,3)\ \mathcal{Y}_i = \exp\left(\frac{E_{b1}+E_{b2}+E_{b3}-E_{bi}}{RT}\right) \qquad \text{(A3)}$$

E_b is calculated using the generalized structure-activity relationship developed by Peeters et al. (2004).

A5 Skill of the model

The evolution of the modelled chemical system can be examined through its instantaneous speciation (Figs. A1). Furthermore, given that the oxidation of CO by HO is negligible in the time scale of experiment, we define the chemical speed of the system, $\mathcal{V}$, as $\frac{d[CO+CO_2]}{dt}$ (Figs. A2). Both proxies indicate that the system undergoes three different regimes:

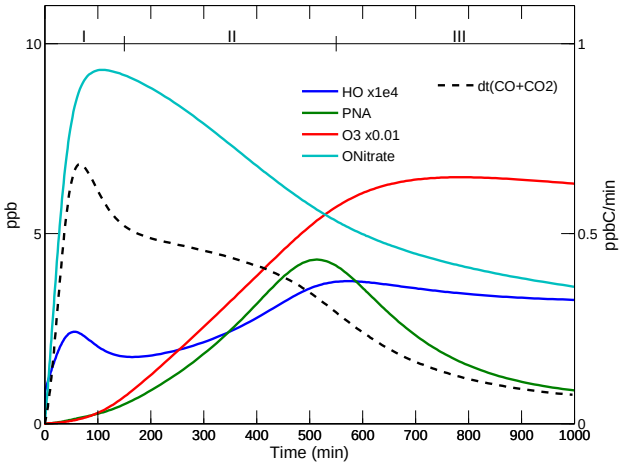

Fig. A2. Different stages of the reaction. Regime I: alkenes chemistry, NO_x-dominated. Regime II: aldehydes chemistry, NO_x-dominated. Regime III: ketones and peroxides chemistry, HO_x-dominated.

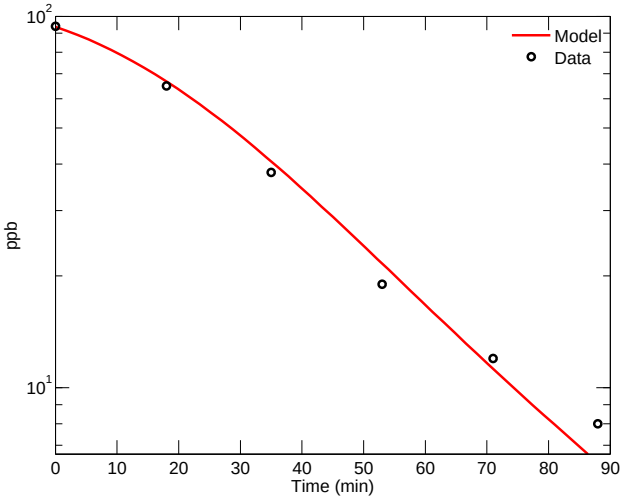

Fig. A3. Isoprene profile monitored by GC FID compared to modeled isoprene.

First regime (0<t<150 min). This regime is characterized by a large supply of NO, as well as very reactive compounds featuring a double bond. $\mathcal{V}$ reaches a maximum after a few minutes at 0.7 ppv(C)/min. O_3 and PNA are very low in this regime, underlying a chemistry dominated by NO. The organic nitrate concentration reaches its maximum at the end of this regime. The reduction in [HO] corresponds to an increase of $[NO_2]$ leading to the formation of nitric acid.

Second regime 150<t<550 min. This regime is characterized by a very stable $\mathcal{V}$ (0.5 ppbv(C)/min) with a chemistry dominated by aldehydes. HO recycling though $HO_2 + NO$ is less efficient than in the first regime due to the abundance of O_3 which favors the formation of PAN. Nevertheless, the reduction in the chemical speed due to the transition from "double bond dominated" to "aldehyde dominated" reduces HO sinks which ultimately leads to a slow increase in HO, leveling off when PNA peaks, i.e. when the NO_x is titrated.

Third regime 550 <t<1000 min. After the PNA peak, the chemistry is dominated by HO_2, as evidenced by the formation of peracetic acid (PAA cluster at m/z=161) and methylhydroperoxide (MHP cluster m/z=133). Low-reactivity compounds such as ketones or long-lived nitrates dominate the chamber composition. Despite the almost constant HO, the chemical speed drops significantly to 0.1 ppbv(C)/min.

These three distinct chemical regimes are consistent with the ones derived using the experimental profiles of HONO and PNA, i.e. the mechanism accurately represents the average evolution of the chemical system (Figs. A1 and A2).

The skill of the mechanism can be evaluated in greater details by comparing the times when various species peak as well as their maxima between mechanism and experiment (Table A1). The mechanism generally captures correctly the peak times indicating that the chemical speed is properly modeled in the first and second regime. The error regarding the maximum intensity falls within the uncertainty of this study ($\pm 20-30\%$). The sensitivity of the CIMS to PNA is probably overevaluated due to ligand exchange with H_2O_2. Satisfactory representation for the background chemistry species is also reached (Figs. A3 and A4). In particular, HO_2NO_2, a very sensitive marker for the ratio of NO_x and HO_x, is well captured during the first and second regimes.

Table A1. Skill of the model. $\Delta t = t_{max}^{model}/t_{max}^{data} - 1$ and $\Delta c = c_{max}^{model}/c_{max}^{data} - 1$.

	HACET	GLYC	ISOPN	MVKN + MACRN	HC5
Δt (%)	4.8	-1.4	< 1	< 1	< 1
Δc_{max} (%)	3.6	−4.4	2.4	−3.1	38
	ETHN	DHB	DHPN	HONO	PNA
Δt (%)	< 1	< 1	2.1	16	-11
Δc_{max} (%)	-11	3.5	22	2.2	-37

Appendix B

Calibration

B1 Definitions

We define the normalized signal, $\widehat{Signal(m/z)}$ as the absolute number of counts recorded at m/z divided by the number

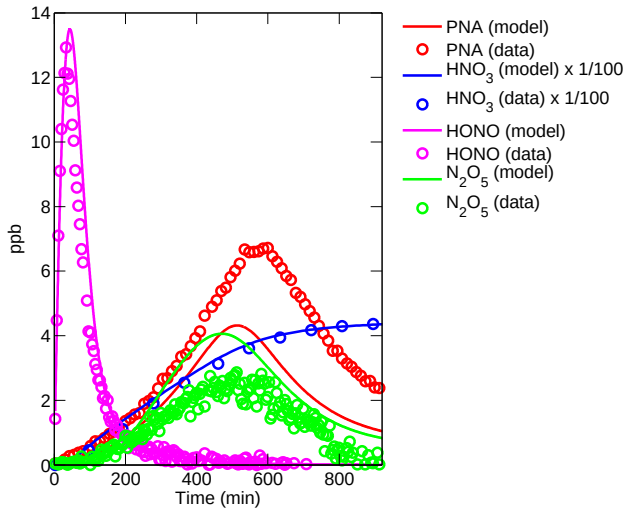

Fig. A4. Comparison of CIMS measurements of inorganic species with their modeled concentrations using experimental calibrations. Calibrations for HO_2NO_2 and N_2O_5 are uncertain.

of counts associated with the reagent anion, CF_3O^-:

$$\widehat{Signal(m/z)} = \frac{Signal(m/z)}{Signal(CF_3O^-)} \quad \text{(B1)}$$

For the chamber experimental conditions, the reagent ion was found in several forms: CF_3O^-, $CF_3O{\cdot}H_2O$ and $CF_3O^-{\cdot}H_2O_2$. Due to the high count rates for the primary isotopes of the reagent ions (sum $\sim$ 14 MHz), the ^{13}C isotopes were monitored instead:

$$Signal(CF_3O^-) = \sum_{m/z=86,104,120} Signal(m/z) \quad \text{(B2)}$$

As stated in Sect. 2.3, in order to get the concentration for an analyte, X, detected as a product ion with m/z=p, we divide the normalized signal for m/z by the sensitivity (c_X) for that analyte under chamber conditions Eq. (1).

The above method fails when mass analog ions, i.e. different ions with the same mass-to-charge ratio, exist at the m/z of interest. The mass analog ions correspond to different analytes in the chamber, which have different reaction rate coefficients with the reagent ion. While the CIMS instrument can not separate mass analogs, the explicit model can. To compare the model results with a measured signal composed of mass analogs, we use the following:

$$\left[X_{\text{measured } m/z=a}\right]_{\text{ppbv}} = \frac{\widehat{Signal(m/z)}}{c_{ref}} \quad \text{(B3)}$$

$$\left[X_{\text{model } m/z=a}\right]_{\text{ppbv}} = \sum_{i\in\mathcal{A}} [X_i] \frac{c_{X_i}}{c_{ref}} \quad \text{(B4)}$$

where a is a m/z featuring mass analog ions, $\mathcal{A}$ the subset of compounds yielding product ions with m/z=a and c_{ref}=3.85×10^{-4} pptv^{-1} is taken as an approximate general calibration. Nominally, Signal(CF_3O^-)=120 kcounts/s, this gives c_{ref}=46 counts.s^{-1}.pptv^{-1}, in the CIMS flow tube. Including the dilution factor (13.2), the sensitivity is 3.5 counts.s^{-1}.pptv^{-1} in the chamber air.

B2 Dipoles and polarizabilities computed by quantum mechanics

The dipole moment and polarizability of a molecule depend on its charge distribution. Thus, different conformers of a molecule can have very different dipole moments. The polarizability is essentially determined by the number of electrons and so is not significantly altered by conformers.

We have calculated the dipole moment and polarizability using density functional theory. Many of the molecules of interest have a large number of structural conformers and we have calculated a conformer distribution for all molecules. To generate the initial set of conformers, we have allowed 3 fold rotation about all CC, CO, CN single bonds. This leads to, for example 34 guess structures in the case of ISOPN Z(1, 4). For each guess conformer, geometry optimization is conducted at the B3LYP/6-31G(d) level. The optimized conformers are ranked by energy and relative population for a temperature of 298 K is determined. We have only calculated the polarizability of the lowest energy structure for each of the molecules as we found this to be relatively insensitive to structure. All calculations were performed with Spartan'06, with the default convergence criteria (Wavefunction Inc., 2006). Test calculations on a few small molecules for which the dipole moment has been measured show that the B3LYP/6-31G(d) calculated dipole moments are in good agreement with experiment (Table B1).

Appendix C

Uncertainty

C1 Initial branching ratio uncertainty

The addition of HO onto isoprene yields eight different peroxyradicals (Fig. 1). The reported branching ratios vary significantly (Lei et al., 2001; Greenwald et al., 2007).

MACR and MVK are only produced through the reaction of the β-hydroxy alkoxy radicals with NO and by ozonolysis of isoprene (Fig. 1). Since the latter accounts for less than 0.5% of the total isoprene consumption in the chamber, we can use the direct determination of the yield of these products (Sprengnether et al., 2002) as a constraint.

$$(1-\alpha_\beta)(Y_{1,2}+Y_{2,1}) = 0.44\pm0.06 \quad \text{(C1)}$$

$$(1-\alpha_\beta)(Y_{4,3}+Y_{3,4}) = 0.28\pm0.04 \quad \text{(C2)}$$

We consider that all β-hydroxy peroxy radical have the same nitrate branching ratio, α_β, as suggested by Giacopelli et al.

(2005). In this study, we assume that channels (2, 1) (respectively (3, 4)) yield MVK and MACR. Park et al. (2003) proposed that the radicals formed in these channels undergo a cyclization, thus reducing the yield of MVK and MACR. The yield of the nitrates which should originate from the hydrocarbons proposed by Park et al. (2003) is too small to provide conclusive experimental evidence in favor or against this mechanism. Given the small combined yield of these channels, this uncertainty remains small compared to the ones affecting the major channels.

Theoretical determinations of the branching ratio have also been made (Lei et al., 2000; Greenwald et al., 2007):

$$Y_{1,2} + Y_{1,4} = 0.56; 0.67 \quad \text{(C3)}$$

$$Y_{4,3} + Y_{4,1} = 0.29; 0.37 \quad \text{(C4)}$$

$$Y_{2,1} = 0.02 \quad \text{(C5)}$$

$$Y_{3,4} = 0.02; 0.05 \quad \text{(C6)}$$

The product of the decomposition of the isoprene nitrates formed in the (4, 1) branch, dihydroxybutanone (DHB) and propanone nitrate (PROPNN), provide an additional constraint (Fig. 8):

$$0.01 < (1-\alpha_{2,1}^{dn})\gamma\alpha_\beta Y_{2,1} + (1-\alpha_{4,1}^{dn})\alpha_\delta Y_{4,1} < 0.034 \quad \text{(C7)}$$
$$\pm 0.002 \qquad\qquad \pm 0.007$$

where α_δ is the nitrate yield from the δ-hydroxy peroxy radicals, γ is the branching ratio of the pathway yielding propanone nitrate from ISOPN(2, 1), computed using (A3), $\alpha_{2,1}^{dn}$ and $\alpha_{4,1}^{dn}$, the respective organic dinitrate branching ratios from ISOPN(2, 1) and ISOPN(4, 1).

The upper and lower bounds reflect the uncertainty on the identification of the m/z=189 signal. The upper bound is derived assuming all $m/$=189 signal originates from the DHB yielded by ISOPN(4, 1). The lower limit assumes that no DHB is formed from ISOPN but rather that the signal measured at m/z=189 results from the photooxidation of HC5 Z(1, 4) (negligible based on Peeters' SAR) and ISOPN (1, 4) (formation of dihydroxymethylpropanal (DHMPL) from addition of HO on the less-sterically favored carbon).

In the mechanism, we use the constraints implied by the study of Lei et al. (2000), Y_{MACR}=0.26 and Y_{MVK}=0.40 and the upper bound of Eq. C7. Since the use of the non linear system formed by Eqs. (C1) to (C7) in order to solve for α_β, α_δ and $Y_{i,j}$ does not yield a single solution, we use the branching ratios derived by Lei et al. (2001) to initialize the numerical solution of this non-linear system and obtain: $Y_{1,2}\simeq$41%, $Y_{1,4}\simeq$15%, $Y_{2,1}\simeq$2%, $Y_{4,3}\simeq$23%, $Y_{4,1}\simeq$14%, $Y_{3,4}\simeq$5%, $\alpha_\delta\simeq$24%, $\alpha_\beta\simeq$6.7%. This set of parameters yields a self-consistent mechanism which captures correctly most of our observations.

The constraints implied by the theoretical study of Greenwald et al. (2007) and the experimental work of Sprengnether et al. (2002) can not be reconciled with our observations in a consistent fashion. Consider the extreme case where Y_{MACR}=24%, $Y_{4,3}+Y_{4,1}$=29% and $Y_{2,1}$=2% and assume a nitrate yield of 10% for the β-hydroxy channels gives $Y_{4,1}\simeq$4.7%. A direct consequence of the small branching ratio for (4, 1) branch is to preclude DHBN from being an important product of ISOPN(4, 1). The signal measured at m/z=189 would therefore mostly correspond to DHMPL formed from the photooxidation of ISOPN(1, 4). There are two major inconsistencies with this hypothesis. First, due to the small carbon flux through the (4, 1) branch, we are not able to capture the prompt source of hydroxyacetone attributed to Dibble mechanism. Second, DHMPL features an aldehydic group so that its lifetime with respect of HO is expected to be much shorter than DHB inconsistent with the signal recorded at m/z=189 (Fig. 12).

Table B1. Weighted average dipoles ($\overline{\mu}$) and polarizabilities (α). Experimental determinations are indicated in parenthesis when available. k_X, is the weighted average of the collision rates calculated for conformers with an abundance greater than 5%. $k_{\mathrm{HNO_3}}$=1.92×10^{-9} cm^3 molecule^{-1} s^{-1} . σ is the weighted standard deviation of the distribution of thermal collision rate constants, i.e. it indicates the sensitivity of the calibration to the calculated distribution of conformers.

Molecule (X)	$\overline{\mu}$(D)	α (Å)	$k_X/k_{\mathrm{HNO_3}}$	σ
Acetic Acid	1.6 (1.7$^\diamond$)	3.9 (5.1$^\circledast$)	0.80 (0.84)	∅
DHB	2.3	7.5	1.0	0.027
DHMOB14	1.5	9.3	0.79	0.26
DHMOB41	1.1	9.1	0.66	0.12
DHPN	1.5	6.0	0.74	∅
ETHLN	2.7	6.2	1.1	0.4
Formic Acid	1.4 (1.4$^\diamond$)	2.4 (3.3$^\diamond$)	0.76 (0.78)	∅
GLYC	2.3 (2.34§)	4.5	1.1 (1.1)	∅
HACET	3.1 (3.1†)	5.5	1.4 (1.4)	0.72×10^{-3}
HC5 E(4, 1)	2.8	8.9	1.2	0.22
HC5 Z(1, 4)	3.5	8.7	1.5	0.14
HC5 Z(4, 1)	3.7	8.9	1.5	∅
HOPL	1.2	5.7	0.65	1.6×10^{-3}
ISOPN (1, 2)	2.5	11	1.0	0.032
ISOPN (2,1)	2.5	11	1.0	0.17
ISOPN (3, 4)	2.4	11	1.0	0.11
ISOPN (4, 3)	2.5	11	1.0	0.068
ISOPN (1, 4)E	3.2	11	1.3	0.17
ISOPN (4, 1)E	2.9	12	1.2	0.085
ISOPN (1, 4)Z	3.2	11	1.3	0.028
ISOPN (4, 1)Z	3.0	11	1.2	0.041
MACRN(m)	2.4	9.9	1.0	0.38
MACRN	2.0	9.8	0.87	0.045
MNBL Z(1, 4)	3.6	11	1.4	0.089
MNBL Z(4, 1)	3.9	12	1.5	0.12
MNBOL Z(1, 4)	4.3	12	1.6	0.073
MNBOL Z(4, 1)	4.2	12	1.6	0.083
MOBA Z(1, 4)	4.6	9.1	1.8	0.22
MOBA Z(4, 1)	3.2	9.2	1.3	∅
MVKN(m)	2.2	9.7	0.95	0.39
MVKN	2.3	9.9	0.95	0.078
PROPNN	3.0	7.7	1.3	0.46
Propanoic Acid	1.5	5.4	0.76	0.034
Pyruvic Acid	2.4	5.5	1.0	∅

$^\diamond$: Johnson III, R. D. (2006), †: Apponi et al. (2006), *: Cox et al. (1971)
$^\circledast$: Maryott and Buckley (1953), §: Marstokk and Mollendal (1973)

While the derivation of the specific branching ratio is affected by this major uncertainty, the determination of the overall yield of the different products identified is, on the other hand, strongly constrained by observations and thus relatively insensitive to our choice. The asymmetry of the nitrate yields between the β and δ-hydroxy channels is therefore a reliable feature. Indeed this conclusion bears a striking similarity with the estimate derived by Giacopelli et al. (2005) using a corrected Carter's parameterization. It is also consistent with the suggestion of O'Brien et al. (1998) that hydrogen bonding in β-hydroxy substituted ROONO intermediate weakens the RO−ONO bond, enhancing $RO + NO_2$ production.

C2 Quantum mechanics

In this study, we have assumed that ligand exchange has a negligible impact on CIMS sensitivity. Therefore to assess the accuracy of our calibration, we compare the calculated collision rate with the fastest experimental collision rate:

$$k_X^r = \frac{c_X^e}{c_{\mathrm{HNO_3}}} k_{\mathrm{HNO_3}}^r \tag{C8}$$

where $k_{\mathrm{HNO_3}}^r = 2.2\times10^{-9}$ cm^3 molecule^{-1} s^{-1} (Huey et al., 1996; Amelynck et al., 2000) and c_X^e is the maximum sensitivity of this technique determined experimentally by changing the water vapor mixing ratio (often found at zero water vapor mixing ratio).

The sensitivity of the CIMS to strong acids (nitric acid ($r=\frac{k_X.k_{\mathrm{HNO_3}}^r}{k_{\mathrm{HNO_3}}k_X^r}=0.9$) or representative VOC (glycolaldehyde, $r=0.85$) appears to be correctly captured using the thermal collision rate. Furthermore in a recent study, Ng et al. (2008) monitored the oxidation of isoprene by NO_3 using CIMS. Using the dipoles and the polarizabilities of MNBOL(1, 4)/(4, 1) ((2Z)-2/3-methyl-4-(nitrooxy)but-2-ene-1-peroxol) and MNBL(1, 4)/(4, 1) ((2Z)-3/2-methyl-4-(nitrooxy)but-2-enal) and ISOPN(4, 1) (Table B1), we infer that they account for 100% of the carbon flux, consistent with previous determination.

Conversely, the sensitivity to smaller molecules such as formic (r=1.5) or acetic acid (r=2) is largely overpredicted. If the experimental rates of Amelynck et al. (2000) are used, the agreement is much better with r=1.0 for formic acid and r=1.1 for acetic acid. The discrepancy may be explained by the smaller collisional energy used in the Amelynck et al. (2000)'s experiment which would result in fewer A^-.HF complexes being broken during the expansion into the high vacuum.

C3 Inorganic chemistry uncertainties

In addition to uncertainties associated with the VOC chemistry, proper modeling of the background chemistry must be achieved to derive conclusions regarding the VOC chemistry. The model is especially sensitive to the following parameters:

Nitric acid. The rate of $HO + NO_2 + M \rightarrow HNO_3$ is an important uncertainty regarding the background chemistry. We use the recently reported rate coefficient of 9.16×10^{-12} cm^3 molecule^{-1} s^{-1} (Okumura and Sander, 2005) which tends to reduce the rate of formation of nitric acid and conversely increases the formation rate of ozone in comparison with the previous estimates (Atkinson et al., 2006).

Dinitrogen Pentoxide. N_2O_5 is known to react with water on surfaces (aerosol, walls) to yield nitric acid:

$$N_2O_5 + H_2O \xrightarrow{\mathcal{S}} 2HNO_3 \tag{R20}$$

The DMA measurements can be used to obtain the aerosol surface area $\mathcal{S}$ and the collision rate, $k_{\mathrm{coll}}=\frac{1}{4}\sqrt{\frac{8RT}{\pi M}}\mathcal{S}=2\times10^{-3}$ cm^3 molecule^{-1} s^{-1} . The accommodation coefficient is set to 0.05.

Initial concentration of H_2O_2. Due to the technique used in this experiment to introduce H_2O_2 into the chamber, its concentration is not known accurately. No calibration is available at such a high hydrogen peroxide level, so that its estimate based on CIMS measurement is uncertain: 1.9–2.3 ppm. A new injection method has been developed to this uncertainty in future studies.

Acknowledgements. The authors wish to thank T. S. Dibble, D. Taraborrelli and an anonymous referee for their helpful comments on the initial manuscript. F. Paulot wishes to thank C. D. Vecitis for helpful discussions regarding chemical mechanisms. This study was supported by the National Science Foundation (NSF) under grant ATM-0432377, by the US Department of Energy under grant DE-FG02-05ER63983, by US Environmental Protection Agency under grant RD-83374901 and by the Marsden Fund administrated by the Royal Society of New Zealand. F. Paulot is supported by the William and Sonya Davidow graduate fellowship. J. D. Crounse thanks the EPA-STAR Fellowship Program (FP916334012) for providing support. This work has not been formally reviewed by the EPA. The views expressed in this document are solely those of the authors and the EPA does not endorse any products or commercial services mentioned in this publication.

Edited by: J. Burkholder

References

Amelynck, C., Schoon, N., and Arijs, E.: Gas phase reactions of CF_3O^- and $CF_3O^-H_2O$ with nitric, formic, and acetic acid, Int. J. Mass Spectrom., 203, 165–175, 2000.

Andreae, M. O., Andreae, T. W., Talbot, R. W., and Harriss, R. C.: Formic and acetic acid over the central Amazon region, Brazil. I-Dry season, J. Geophys. Res., 93, 1616–1624, 1988.

Apponi, A. J., Hoy, J. J., Halfen, D. T., Ziurys, L. M., and Brewster, M. A.: Hydroxyacetone (CH_3COCH_2OH): a combined microwave and millimeter-wave laboratory study and associated astronomical search, The Astrophysical Journal, 652, 1787–1795, 2006.

Arey, J., Aschmann, S. M., Kwok, E. S. C., and Atkinson, R.: Alkyl nitrate, hydroxyalkyl nitrate, and hydroxycarbonyl formation from the NO_x-air photooxidations of C_5-C_8 n-alkanes, J. Phys. Chem. A., 105, 1020–1027, 2001.

Atkinson, R.: Gas-phase tropospheric chemistry of volatile organic compounds: 1. Alkanes and Alkenes, Journal of Physical and Chemical Reference Data, 26, 215–290, 1997.

Atkinson, R., Aschmann, S. M., Tuazon, E. C., Arey, J., and Zielinska, B.: Formation of 3-Methylfuran from the gas-phase reaction of OH radicals with isoprene and the rate constant for its reaction with the OH radical, Int. J. Chem. Kin., 21, 593–604, 1989.

Atkinson, R., Baulch, D. L., Cox, R. A., Crowley, J. N., Hampson, R. F., Hynes, R. G., Jenkin, M. E., Rossi, M. J., and Troe, J.: Evaluated kinetic and photochemical data for atmospheric chemistry: Volume I-gas phase reactions of O_x, HO_x, NO_x and SO_x species, Atmos. Chem. Phys., 4, 1461–1738, 2004, http://www.atmos-chem-phys.net/4/1461/2004/.

Atkinson, R., Baulch, D. L., Cox, R. A., Crowley, J. N., Hampson, R. F., Hynes, R. G., Jenkin, M. E., Rossi, M. J., and Troe, J.: Evaluated kinetic and photochemical data for atmospheric chemistry: Volume II–gas phase reactions of organic species, Atmos. Chem. Phys., 6, 3625–4055, 2006, http://www.atmos-chem-phys.net/6/3625/2006/.

Atkinson, R., Arey, J., and Aschmann, S.: Atmospheric chemistry of alkanes: Review and recent developments, Atmos. Environ., 42, 5859–5871, 2008.

Baker, J., Arey, J., and Atkinson, R.: Formation and reaction of hydroxycarbonyls from the reaction of OH radicals with 1,3-butadiene and isoprene, Environ. Sci. Technol., 39, 4091–4099, 2005.

Bethel, H. L., Atkinson, R., and Arey, J.: Kinetics and products of the reactions of selected diols with the OH radical, Int. J. Chem. Kin., 33, 310–316, 2001.

Bierbach, A., Barnes, I., and Becker, K. H.: Product and kinetic study of the OH-initiated gas-phase oxidation of furan, 2-methylfuran and furanaldehydes at $\simeq$300 K, Atmos. Environ., 29, 2651–2660, 1995.

Butkovskaya, N. I., Pouvesle, N., Kukui, A., and Bras, G. L.: Mechanism of the OH-initiated oxidation of glycolaldehyde over the temperature range 233-296 K., J. Phys. Chem. A., 110, 13 492–13 499, 2006a.

Butkovskaya, N. I., Pouvesle, N., Kukui, A., Mu, Y., and Le Bras, G.: Mechanism of the OH-initiated oxidation of hydroxyacetone over the temperature range 236-298 K, J. Phys. Chem. A., 110, 6833–6843, 2006b.

Cameron, M., Sivakumaran, V., Dillon, T. J., and Crowley, J. N.: Reaction between OH and CH3CHO Part 1. Primary product yields of CH_3 (296 K), CH_3CO (296 K), and H (237–296 K), Phys. Chem. Chem. Phys., 4, 3628–3638, 2002.

Carlton, A. G., Turpin, B. J., Lim, H. J., Altieri, K. E., and Seitzinger, S.: Link between isoprene and secondary organic aerosol (SOA): Pyruvic acid oxidation yields low volatility organic acids in clouds, Geophys. Res. Lett, 33, L06822, doi: 10.1029/2005GL025374, 2006.

Carter, W. P. L. and Atkinson, R.: Alkyl nitrate formation from the atmospheric photoxidation of alkanes; a revised estimation method, J. Amos. Chem., 8, 165–173, 1989.

Chameides, W. L., Lindsay, R. W., Richardson, J., and Kiang, C. S.: The role of biogenic hydrocarbons in urban photochemical smog: Atlanta as a case study, Science, 241, 1473, doi:10.1126/science.3420404, 1988.

Chebbi, A. and Carlier, P.: Carboxylic acids in the troposphere, occurrence, sources, and sinks: A review, Atmos. Environ., 30, 4233–4249, 1996.

Chen, X., Hulbert, D., and Shepson, P. B.: Measurement of the organic nitrate yield from OH reaction with isoprene, J. Geophys. Res., 103, 25 563–25 568, 1998.

Chuong, B. and Stevens, P. S.: Measurements of the kinetics of the OH-initiated oxidation of isoprene, J. Geophys. Res, 107, 4162, doi:{10.1029/2001JD000865}, 2002.

Chuong, B. and Stevens, P. S.: Measurements of the kinetics of the OH-initiated oxidation of methyl vinyl ketone and methacrolein, Int. J. Chem. Kin., 36, 12–25, 2004.

Claeys, M., Graham, B., Vas, G., Wang, W., Vermeylen, R., Pashynska, V., Cafmeyer, J., Guyon, P., Andreae, M. O., Artaxo, P., et al.: Formation of secondary organic aerosols through photooxidation of isoprene, Science, 303, 1173–1176, 2004.

Cox, A. P., Brittain, A. H., and Finnigan, D. J.: Microwave spectrum, structure, dipole moment and quadrupole coupling constants of cis and trans nitrous acids, Trans. Faraday Soc., 67, 2179–2194, 1971.

Crounse, J. D., McKinney, K. A., Kwan, A. J., and Wennberg, P. O.: Measurement of gas-phase hydroperoxides by chemical ionization mass spectrometry, Anal. Chem., 78, 6726–6732, 2006.

Dibble, T.: Cyclization of 1, 4-hydroxycarbonyls is not a homogenous gas phase process, Chem. Phys. Lett., 447, 5–9, 2007.

Dibble, T. S.: Isomerization of OH-isoprene adducts and hydroxyalkoxy isoprene radicals, J. Phys. Chem. A., 106, 6643–6650, 2002.

Dibble, T. S.: Intramolecular hydrogen bonding and double H-atom transfer in peroxy and alkoxy radicals from isoprene, J. Phys. Chem. A., 108, 2199–2207, 2004a.

Dibble, T. S.: Prompt chemistry of alkenoxy radical products of the double H-atom transfer of alkoxy radicals from isoprene, J. Phys. Chem. A., 108, 2208–2215, 2004b.

Dillon, T. J., Horowitz, A., Hölscher, D., Crowley, J. N., Vereecken, L., Peeters, J., and Matter, S.: Reaction of HO with hydroxyacetone ($HOCH_2C(O)CH_3$): rate coefficients (233–363 K) and mechanism, Phys. Chem. Chem. Phys., 8, 236–246, 2006.

Duce, R. A., LaRoche, J., Altieri, K., Arrigo, K. R., Baker, A. R., Capone, D. G., Cornell, S., Dentener, F., Galloway, J., Ganeshram, R. S., et al.: Impacts of atmospheric anthropogenic nitrogen on the open ocean, Science, 320, 893–897, doi: 10.1126/science.1150369, 2008.

Fan, J. and Zhang, R.: Atmospheric Oxidation Mechanism of Isoprene, Environ. Chem., 1, 140–149, 2004.

Fiore, A. M., Horowitz, L. W., Purves, D. W., II, H. L., Evans, M. J., Wang, Y., Li, Q., and Yantosca, R. M.: Evaluating the contribution of changes in isoprene emissions to surface ozone trends over the eastern United States, J. Geophys. Res., 110, D12303, doi:{10.1029/2004JD005485}, 2005.

Francisco-Marquez, M., Alvarez-Idaboy, J. R., Galano, A., and Vivier-Bunge, A.: A possible mechanism for furan formation in the tropospheric oxidation of dienes, Environ. Sci. Technol., 39, 8797–8802, 2005.

Giacopelli, P., Ford, K., Espada, C., and Shepson, P. B.: Comparison of the measured and simulated isoprene nitrate distributions above a forest canopy, J. Geophys. Res., 110, D01304,

doi:10.1029/2004JD005123, 2005.

Greenwald, E., North, S., Georgievskii, Y., and Klippenstein, S.: A two transition state model for radical-molecule reactions: applications to isomeric branching in the OH-isoprene reaction, J. Phys. Chem. A., 111, 5582–5592, 2007.

Guenther, A., Karl, T., Harley, P., Wiedinmyer, C., Palmer, P. I., and Geron, C.: Estimates of global terrestrial isoprene emissions using MEGAN (Model of Emissions of Gases and Aerosols from Nature), Atmos. Chem. Phys., 6, 3181–3210, 2006, http://www.atmos-chem-phys.net/6/3181/2006/.

Harley, P., Vasconcellos, P., Vierling, L., Pinheiro, C. C., Greenberg, J., Guenther, A., Klinger, L., Almeida, S. S., Neill, D., Baker, T., et al.: Variation in potential for isoprene emissions among neotropical forest sites, Glob. Change Biol., 10, 630–650, 2004.

Harley, P. C., Monson, R. K., and Lerdau, M. T.: Ecological and evolutionary aspects of isoprene emission from plants, Oecologia, 118, 109–123, 1999.

Hasson, A. S., Tyndall, G. S., and Orlando, J. J.: A product yield study of the reaction of HO_2 radicals with ethyl peroxy ($C_2H_5O_2$), acetyl peroxy ($CH_3C(O)O_2$), and acetonyl peroxy ($CH_3C(O)CH_2O_2$) radicals, J. Phys. Chem., 108, 5979–5989, 2004.

Henze, D. K. and Seinfeld, J. H.: Global secondary organic aerosol from isoprene oxidation, Geophys. Res. Lett., 33, L09812, doi:{10.1029/2006GL025976}, 2006.

Hermans, I., Müller, J. F., Nguyen, T. L., Jacobs, P., and Peeters, J.: Kinetics of α-hydroxy-alkylperoxyl radicals in oxidation processes. HO_2 initiated oxidation of ketones/aldehydes near the tropopause, J. Phys. Chem. A., 109, 4303–4311, 2005.

Horowitz, L. W., Liang, J., Gardner, G. M., and Jacob, D. J.: Export of reactive nitrogen from North America during summertime-Sensitivity to hydrocarbon chemistry, J. Geophys. Res., 103, 13 451–13 476, 1998.

Horowitz, L. W., Fiore, A. M., Milly, G. P., Cohen, R. C., Perring, A., Wooldridge, P. J., Hess, P. G., Emmons, L. K., and Lamarque, J.: Observational constraints on the chemistry of isoprene nitrates over the eastern United States, J. Geophys. Res., 112(12), D12S08, doi:10.1029/2006JD007747, 2007.

Huey, L. G., Villalta, P. W., Dunlea, E. J., Hanson, D. R., and Howard, C. J.: Reactions of CF_3O^- with atmospheric trace gases, J. Phys. Chem., 100, 190–194, 1996.

Jacob, D. J. and Wofsy, S. C.: Photochemistry of biogenic emissions over the Amazon forest, J. Geophys. Res., 93, 1477–1486, 1988.

Jenkin, M. E., Hurley, M. D., and Wallington, T. J.: Investigation of the radical product channel of the $CH_3C(O)O_2 + HO_2$ reaction in the gas phase, Phys. Chem. Chem. Phys., 9, 3149–3162, 2007.

Johnson III, R. D.: NIST Computational Chemistry Comparison and Benchmark Database NIST Standard Reference Database Number 101 Release 14, http://srdata.nist.gov/cccbdb, 2006.

Karl, M., Dorn, H. P., Holland, F., Koppmann, R., Poppe, D., Rupp, L., Schaub, A., and Wahner, A.: Product study of the reaction of OH radicals with isoprene in the atmosphere simulation chamber SAPHIR, J. Amos. Chem., 55, 167–187, 2006.

Karunanandan, R., Hölscher, D., Dillon, T. J., Horowitz, A., Crowley, J. N., Vereecken, L., and Peeters, J.: Reaction of HO with Glycolaldehyde, $HOCH_2CHO$: Rate Coefficients (240–362 K) and Mechanism, J. Phys. Chem. A., 111, 897–908, 2007.

Kroll, J. H., Ng, N. L., Murphy, S. M., Flagan, R. C., and Seinfeld, J. H.: Secondary organic aerosol formation from isoprene photooxidation, Environ. Sci. Technol, 40, 1869–1877, 2006.

Kwok, E. S. C. and Atkinson, R.: Estimation of hydroxyl radical reaction rate constants for gas-phase organic compounds using a structure-reactivity relationship: an update, Atmos. Environ., 29, 1685–1695, 1995.

Lei, W., Zhang, R., Sean McGivern, W., Derecskei-Kovacs, A., and North, S.: Theoretical study of isomeric branching in the isoprene–OH reaction: implications to final product yields in isoprene oxidation, Chem. Phys. Lett., 326, 109–114, 2000.

Lei, W., Zhang, R., McGivern, W. S., Derecskei-Kovacs, A., and North, S. W.: Theoretical study of $OH - O_2$-isoprene peroxy radicals, J. Phys. Chem. A., 105, 471–477, 2001.

Marstokk, K. and Mollendal, H.: Microwave spectra of isotopic glycolaldehydes, substitution structure, intramolecular hydrogen bond and dipole moment, J. Molecular Struct., 16, 259–270, 1973.

Maryott, A. A. and Buckley, F.: US National Bureau of Standards Circular No. 537, National Bureau of Standards, Washington, DC, 1953.

Méreau, R., Rayez, M. T., Rayez, J. C., Caralp, F., and Lesclaux, R.: Theoretical study on the atmospheric fate of carbonyl radicals: kinetics of decomposition reactions, Phys. Chem. Chem. Phys., 3, 4712–4717, 2001.

Neeb, P.: Structure-reactivity based estimation of the rate constants for hydroxyl radical reactions with hydrocarbons, J. Amos. Chem., 35, 295–315, 2000.

Neeb, P., Sauer, F., Horie, O., and Moortgat, G. K.: Formation of hydroxymethyl hydroperoxide and formic acid in alkene ozonolysis in the presence of water vapour, Atmos. Environ., 31, 1417–1423, 1997.

Ng, N. L., Kwan, A. J., Surratt, J. D., Chan, A. W. H., Chhabra, P. S., Sorooshian, A., Pye, H. O. T., Crounse, J. D., Wennberg, P. O., Flagan, R. C., and Seinfeld, J. H.: Secondary organic aerosol (SOA) formation from reaction of isoprene with nitrate radicals (NO_3), Atmos. Chem. Phys., 8, 4117–4140, 2008, http://www.atmos-chem-phys.net/8/4117/2008/.

O'Brien, J. M., Czuba, E., Hastie, D. R., Francisco, J. S., and Shepson, P. B.: Determination of the hydroxy nitrate yields from the reaction of C_2–C_6 alkenes with OH in the presence of NO, J. Phys. Chem. A., 102, 8903–8908, 1998.

Okumura, M. and Sander, S. P.: Gas-phase formation rates of nitric acid and its isomers under urban conditions, California Environmental Protection Agency, Air Ressources Board, 2005.

Orlando, J. J. and Tyndall, G. S.: The atmospheric chemistry of the HC (O) CO radical, Int. J. Chem. Kin., 33, 149–156, 2001.

Orlando, J. J., Tyndall, G. S., Bertman, S. B., Chen, W., and Burkholder, J. B.: Rate coefficient for the reaction of OH with $CH_2 = C(CH_3)C(O)OONO_2$ (MPAN), Atmos. Environ., 36, 1895–1900, 2002.

Papagni, C., Arey, J., and Atkinson, R.: Rate constants for the gas-phase reactions of OH radicals with a series of unsaturated alcohols, Int. J. Chem. Kin., 33, 142–147, 2001.

Park, J., Stephens, J. C., Zhang, R., and North, S. W.: Theoretical study of the alkoxy radicals derived from isoprene: pressure-and temperature-dependent decomposition rates, J. Phys. Chem. A., 107, 6408–6414, 2003.

Park, J., Jongsma, C. G., Zhang, R., and North, S. W.: OH/OD Initiated Oxidation of Isoprene in the Presence of O_2 and NO, J. Phys. Chem. A., 108, 10 688–10 697, 2004.

Patchen, A. K., Pennino, M. J., Kiep, A. C., and Elrod, M. J.: Direct kinetics study of the product-forming channels of the reaction of isoprene-derived hydroxyperoxy radicals with NO, Int. J. Chem. Kin., 39, 353–361, 2007.

Paulson, S. and Seinfeld, J.: Development and evaluation of a photooxidation mechanism for isoprene, J. Geophys. Res., 97, 20 703–20 715, doi:10.1029/92JD01914, 1992.

Paulson, S. E., Flagan, R. C., and Seinfeld, J. H.: Atmospheric photooxidation of isoprene. I: The hydroxyl radical and ground state atomic oxygen reactions, Int. J. Chem. Kin., 24, 79–101, 1992.

Peeters, J., Vereecken, L., and Fantechi, G.: The detailed mechanism of the OH-initiated atmospheric oxidation of α-pinene: a theoretical study, Phys. Chem. Chem. Phys., 3, 5489–5504, 2001.

Peeters, J., Fantechi, G., and Vereecken, L.: A Generalized Structure-Activity Relationship for the Decomposition of (Substituted) Alkoxy Radicals, J. Amos. Chem., 48, 59–80, 2004.

Pfister, G. G., Emmons, L. K., Hess, P. G., Lamarque, J. F., Orlando, J. J., Walters, S., Guenther, A., Palmer, P. I., and Lawrence, P. J.: Contribution of isoprene to chemical budgets: A model tracer study with the NCAR CTM MOZART-4, J. Geophys. Res., 113, D05308, doi:{10.1029/2007JD008948}, 2008.

Roberts, J. M. and Fajer, R. W.: UV absorption cross sections of organic nitrates of potential atmospheric importance and estimation of atmospheric lifetimes, Environ. Sci. Technol., 23, 945–951, 1989.

Rosenstiel, T. N., Potosnak, M. J., Griffin, K. L., Fall, R., and Monson, R. K.: Increased CO_2 uncouples growth from isoprene emission in an agriforest ecosystem, Nature, 421, 256–259, 2003.

Sander, S.: Chemical kinetics and photochemical data for use in atmospheric studies evaluation number 15, National Aeronautics and Space Administration, Jet Propulsion Laboratory, California Institute of Technology, 2006.

Sanderson, M. G., Jones, C. D., Collins, W. J., Johnson, C. E., and Derwent, R. G.: Effect of climate change on isoprene emissions and surface ozone levels, Geophys. Res. Lett., 30, 1936, doi:10.1029/2003GL017642, 2003.

Saunders, S. M., Jenkin, M. E., Derwent, R. G., and Pilling, M. J.: Protocol for the development of the Master Chemical Mechanism, MCM v3 (Part A): Tropospheric degradation of non-aromatic volatile organic compounds, Atmos. Chem. Phys., 3, 161–180, 2003, http://www.atmos-chem-phys.net/3/161/2003/.

Shallcross, D. E. and Monks, P. S.: New Directions: A role for isoprene in biosphere–climate–chemistry feedbacks, Atmos. Env., 34, 1659–1660, 2000.

Sprengnether, M., Demerjian, K. L., Donahue, N. M., and Anderson, J. G.: Product analysis of the OH oxidation of isoprene and 1, 3-butadiene in the presence of NO, J. Geophys. Res., 107, 8–8, 2002.

Su, T. and Chesnavich, W. J.: Parametrization of the ion–polar molecule collision rate constant by trajectory calculations, J. Chem. Phys., 76, 5183–5185, doi:10.1063/1.442828, 1982.

Surratt, J. D., Murphy, S. M., Kroll, J. H., Ng, N. L., Hildebrandt, L., Sorooshian, A., Szmigielski, R., Vermeylen, R., Maenhaut, W., Claeys, M., et al.: Chemical composition of secondary organic aerosol formed from the photooxidation of isoprene, J. Phys. Chem. A., 110, 9665–9690, 2006.

Talbot, R. W., Andreae, M. O., Berresheim, H., Jacob, D. J., and Beecher, K. M.: Sources and sinks of formic, acetic, and pyruvic acids over Central Amazonia: 2. Wet season, J. Geophys. Res., 95, 799–16, 1990.

Talbot, R. W., Mosher, B. W., Heikes, B. G., Jacob, D. J., Munger, J. W., Daube, B. C., Keene, W. C., Maben, J. R., and Artz, R. S.: Carboxylic acids in the rural continental atmosphere over the eastern United States during the Shenandoah Cloud and Photochemistry Experiment, J. Geophys. Res., 100, 9335–9344, 1995.

Tuazon, E. C. and Atkinson, R.: A product study of the gas-phase reaction of isoprene with the OH radical in the presence of NO, Int. J. Chem. Kin., 22, 1221–1236, 1990.

van Donkelaar, A., Martin, R. V., Park, R. J., Heald, C. L., Fu, T. M., Liao, H., and Guenther, A.: Model evidence for a significant source of secondary organic aerosol from isoprene, Atmos. Environ., 41, 1267–1274, 2007.

von Kuhlmann, R., Lawrence, M. G., Pöschl, U., and Crutzen, P. J.: Sensitivities in global scale modeling of isoprene, Atmos. Chem. Phys., 4, 1–17, 2004, http://www.atmos-chem-phys.net/4/1/2004/.

Wall, K. J., Schiller, C. L., and Harris, G. W.: Measurements of the HONO photodissociation constant, J. Amos. Chem., 55, 31–54, 2006.

Walser, M. L., Park, J., Gomez, A. L., Russell, A. R., and Nizkorodov, S. A.: Photochemical aging of secondary organic aerosol particles generated from the oxidation of d-limonene, J. Phys. Chem. A., 111, 1907–1913, 2007.

Wavefunction Inc.: Spartan'06, 2006.

Wiedinmyer, C., Tie, X., Guenther, A., Neilson, R., and Granier, C.: Future changes in biogenic isoprene emissions: How might they affect regional and global atmospheric chemistry?, Earth Interactions, 10, 1–19, 2006.